Argonaute NRDE-3 and MBT domain protein LIN-61 redundantly recruit an H3K9me3 HMT to prevent embryonic lethality and transposon expression

Jan Padeken,[1] Stephen Methot,[1] Peter Zeller,[1,2,3] Colin E. Delaney,[1] Veronique Kalck,[1] and Susan M. Gasser[1,2]

[1]Friedrich Miescher Institute for Biomedical Research, CH-4058 Basel, Switzerland; [2]Faculty of Natural Sciences, University of Basel, CH-4056 Basel, Switzerland

The establishment and maintenance of chromatin domains shape the epigenetic memory of a cell, with the methylation of histone H3 lysine 9 (H3K9me) defining transcriptionally silent heterochromatin. We show here that the *C. elegans* SET-25 (SUV39/G9a) histone methyltransferase (HMT), which catalyzes H3K9me1, me2 and me3, can establish repressed chromatin domains de novo, unlike the SETDB1 homolog MET-2. Thus, SET-25 is needed to silence novel insertions of RNA or DNA transposons, and repress tissue-specific genes de novo during development. We identify two partially redundant pathways that recruit SET-25 to its targets. One pathway requires LIN-61 (L3MBTL2), which uses its four MBT domains to bind the H3K9me2 deposited by MET-2. The second pathway functions independently of MET-2 and involves the somatic Argonaute NRDE-3 and small RNAs. This pathway targets primarily highly conserved RNA and DNA transposons. These redundant SET-25 targeting pathways (MET-2–LIN-61–SET-25 and NRDE-3–SET-25) ensure repression of intact transposons and de novo insertions, while MET-2 can act alone to repress simple and satellite repeats. Removal of both pathways in the *met-2;nrde-3* double mutant leads to the loss of somatic H3K9me2 and me3 and the synergistic derepression of transposons in embryos, strongly elevating embryonic lethality.

[*Keywords*: heterochromatin; HMT; histone methyltransferases (HMTs); SET-25; MET-2; Argonaute; NRDE-3; transposon silencing; LIN-61; MBT domain proteins]

Supplemental material is available for this article.

Received August 27, 2020; revised version accepted November 5, 2020.

About half of our genome consists of repetitive elements. Both transposable elements (Bourque et al. 2018; Klein and O'Neill 2018) and simple repeats are intrinsically unstable and represent a constant threat to genome integrity (Horard et al. 2009; Padeken et al. 2015; Payer and Burns 2019; Khristich and Mirkin 2020) and development (Jachowicz et al. 2017). To counteract the threat of unstable satellite repeats and to prevent the unchecked amplification of transposons, cells must establish and maintain a repressive chromatin structure that blocks transcription of these elements (Slotkin and Martienssen 2007; Deniz et al. 2019). Histone H3 lysine 9 methylation (H3K9me) is associated with constitutively repressed heterochromatin, and it is essential for the silencing of repeats (Nakayama et al. 2001; Peters et al. 2001; Matsui et al. 2010; Allshire and Madhani 2018). In *C. elegans,* the loss of H3K9me, which is achieved by the ablation of its two H3K9 HMTs, SET-25 and MET-2, results in an inappropriate transcription of repetitive elements, which drives genomic instability due to small insertions, deletions, and transposition events (Zeller et al. 2016; Padeken et al. 2019).

In mammals, the loss of H3K9me augments chromosome missegregation and is embryonic lethal (Peters et al. 2001; Tachibana et al. 2002; Dodge et al. 2004). Repeat element transcription, as well as the derepression of pluripotency genes, is commonly observed in a wide range of epithelial cancers (Rodríguez-Paredes and Esteller 2011; Avgustinova et al. 2018; Rowbotham et al. 2018; Ghandi et al. 2019). Further, the inhibition of H3K9 HMTs

[3]Present address: Hubrecht Institute, NL-3584 CT Utrecht, the Netherlands.
Corresponding author: susan.gasser@fmi.ch
Article published online ahead of print. Article and publication date are online at http://www.genesdev.org/cgi/doi/10.1101/gad.344234.120. Freely available online through the *Genes & Development* Open Access option.

facilitates dedifferentiation during the induction of pluripotent stem cells (Soufi et al. 2012; Sridharan et al. 2013; Torrano et al. 2019), and correlates with the derepression of H3K9me-marked tissue-specific genes (Becker et al. 2016).

Thus, from the simplest to the most complex multicellular animal the appropriate establishment of H3K9me-marked domains is critical both for cell identity and genome integrity. Unlike many epigenetic modifications, the establishment of H3K9me2/me3-marked heterochromatin is sufficient to induce a feedback loop that maintains heterochromatic domains through mitotic division once they have been established (Audergon et al. 2015; Ragunathan et al. 2015b; Reinberg and Vales 2018). The crucial question in the field, therefore, is how HMTs are recruited to their target sites either for the establishment or for the maintenance of transcriptional repression (Yamada et al. 2005; Zhang et al. 2008; Fischer et al. 2009; Elgin and Reuter 2013).

Several pathways have already been proposed to recruit HMTs to target sites. One means is to link the HMT catalytic domain to a methyl-lysine "reader" motif. For example, in fission yeast, flies, and mammals, the HMT Su(var) 3-9/SUV39 can bind its own product at pericentric heterochromatin through an N-terminal chromodomain (Allshire and Madhani 2018). In addition, Su(var)3-9/SUV39 interacts with heterochromatin protein 1 (HP1), which itself harbors a chromodomain that binds H3K9me3 (Bannister et al. 2001; Lachner et al. 2001). A second mechanism observed in mammals depends on the sequence-specific binding of KRAB-Zinc finger proteins, which recruit the HMT SETDB1 through TRIM28/KAP1 to silence retrotransposons (Wolf and Goff 2009; Rowe et al. 2010). Other transcription factors have been reported to interact with the G9a HMT in mammals (Shankar et al. 2013). Finally, in fission yeast, siRNAs derived from centromeric satellite repeats bound to an Argonaute can recruit the Clr4 methyltransferase complex (CLRC) to maintain and establish pericentric heterochromatin (Zhang et al. 2008; Holoch and Moazed 2015; Ragunathan et al. 2015a). This Argonaute-RNA pathway resembles the piRNA pathway found in germlines of metazoans (Ozata et al. 2019), in which gonad-specific Argonautes help to repress transposons during meiosis in order to stabilize the germline (Lin and Spradling 1997; Cox et al. 1998; Kuramochi-Miyagawa et al. 2001, 2004; Carmell et al. 2007; Houwing et al. 2007; Tóth et al. 2016; Luo and Lu 2017; van den Beek et al. 2018).

In contrast to yeast, most animals have multiple H3K9 HMTs that show partial redundancy; e.g., SETDB1 and SUV3-9H1 and SUV39H2 at interspersed transposons in mice (Peters et al. 2001; Bulut-Karslioglu et al. 2014) or G9a and GLP for differentiation-specific genes (Collins and Cheng 2010). However, due to chromosome mis-segregation and the early embryonic lethality of HMT mutants (Peters et al. 2001; Tachibana et al. 2002; Dodge et al. 2004; Padeken et al. 2015), it has been difficult to determine whether they have distinct mechanisms of recruitment and whether their redundancy is biologically relevant. *C. elegans* provides a fruitful system to address these questions for the segregation of the worm's holocentric chromosomes is not affected by the loss of H3K9me (Zeller et al. 2016) and worms have only two somatic H3K9 HMTs. Moreover, the *met-2 set-25* double mutant embryos that are devoid of somatic H3K9me can develop into adults, although they show sterility at 25–26°C (Towbin et al. 2012; Garrigues et al. 2015; Zeller et al. 2016). Together with the fact that endogenous *C. elegans* repeat elements are not in large arrays, allowed us to precisely map histone modifications and repeat transcript abundance in single and double H3K9 HMT mutants (Zeller et al. 2016; McMurchy et al. 2017; Ahringer and Gasser 2018; Padeken et al. 2019). We found that both MET-2-mediated H3K9me2 and SET-25-mediated H3K9me3 are able to repress transcription, yet each HMT preferentially silences a distinct class of repetitive elements. MET-2, but not SET-25, is essential for the silencing of simple and satellite repeats and aberrant transcription of those repeats is sufficient to drives the loss of fertility (Garrigues et al. 2015; Zeller et al. 2016; McMurchy et al. 2017; Padeken et al. 2019). The distinct phenotypes of H3K9 HMT single mutants (Padeken et al. 2019) suggested to us that their pathways of recruitment might also be highly divergent.

Using a reporter assay, we have found that only one of the two *C. elegans* H3K9 HMTs, i.e., SET-25, is able to establish a repressive H3K9me domain de novo. A screen for the recruitment of SET-25 to a repetitive reporter implicates two redundant pathways that target SET-25 to chromatin. One pathway depends on the MET-2-mediated H3K9me2 modification, while the second is detectable only in its absence. In the former, we show that the malignant brain tumor (MBT) domain protein LIN-61/L3MBT2L (Bonasio et al. 2010) mediates the recruitment of SET-25 to sites of MET-2-mediated H3K9me2. In the second, SET-25 is targeted to intact RNA and DNA transposons independently of MET-2 through endogenous small RNAs and the somatic Argonaute protein NRDE-3. Loss of one or the other pathway has mild phenotypes on somatic development, but the combined deletion of *met-2* and *nrde-3* synergistically derepresses intact transposons. This, when combined with the derepression of simple repeats, strongly enhanced embryonic lethality. Thus, we describe an essential interplay between two parallel pathways that establish and propagate H3K9me3-mediated repression, and we show that these protect the genome from toxic transposon activation.

Results

H3K9 HMT SET-25, but not MET-2, is sufficient to establish heterochromatin de novo

Mass spectroscopy and immunostaining experiments have shown that the HMT SET-25 is responsible for all H3K9me3 in *C. elegans* somatic tissues, while MET-2 (SETDB1) mediates H3K9me1 and most H3K9me2 (Towbin et al. 2012; Zeller et al. 2016; Padeken et al. 2019). Either dimethylation or trimethylation on H3K9 is able to repress transcription in worms, and thus MET-2 is able

to compensate for the loss of SET-25, by replacing H3K9me3 with H3K9me2 (Fig. 1A; Towbin et al. 2012; Padeken et al. 2019). The opposite is not true. The *met-2 set-25* double mutant lacks all H3K9me, and the *met-2* single mutant loses all but 10%–15% of its H3K9me-marked sequences (Towbin et al. 2012; Garrigues et al. 2015; Padeken et al. 2019). The presence of this residual SET-25 mediated modification, that is, H3K9me3, confirms that SET-25 can generate heterochromatin independently of MET-2. Thus we were driven to ask, what differentiates the two H3K9 HMTs? Why retain both SET-25 and MET-2 in worms?

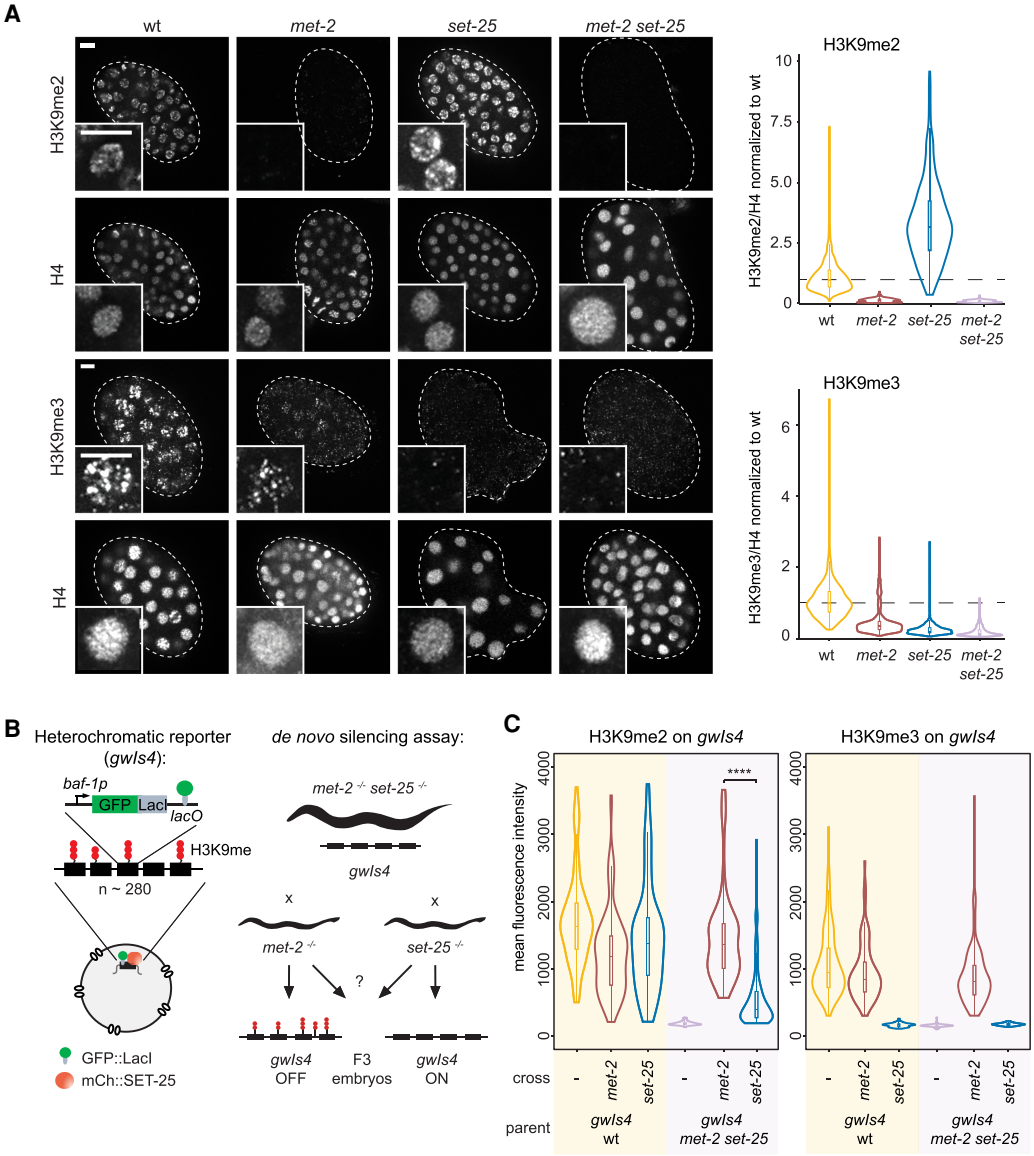

Figure 1. SET-25 is required for de novo establishment of H3K9me2/me3. (*A*) Immunofluorescence and quantitation of H3K9me2, H3K9me3 and H4 in wt, *met-2(n4256)*, set-25(n5021) and *met-2(n4256) set-25(n5021)* embryos, hereafter referred to as *met-2*, *set-25*, and *met-2 set-25*. Fluorescence intensity was normalized to H4. Signal quantified by automated image analysis. For H3K9me2, $N = 2$; wt $n = 1917$, *met-2* $n = 1088$, *set-25* $n = 1177$, *met-2 set-25* $n = 1021$. For H3K9me3, $N = 3$; wt $n = 1467$, *met-2* $n = 851$, *set-25* $n = 1958$, *met-2 set-25* $n = 1405$. Scale bar, 5 µm. (*B*) Scheme of the heterochromatic reporter (*gwIs4*) and de novo silencing assay. The reporter *gwIs4 [baf-1p::GFP-lacI::let-858 3′UTR; myo-3p::RFP]*, is integrated in a single site as an array of ~280 tandem copies. Each copy carries a single lacO site that allows visualization of the array (Meister et al. 2010). To assay maintenance of repression, wild-type hermaphrodites bearing *gwIS4* were crossed with *met-2* or *set-25* mutants and for de novo silencing adult *met-2 set-25* double mutants bearing *gwIS4* were crossed with either *met-2* or *set-25* single mutants. Embryos of the F2 generation homozygous for the *gwIs4* reporter and either the *met-2* or *set-25* deletion were scored for colocalization of H3K9me2, H3K9me3, and GFP. (*C*) Quantitation of the mean H3K9me2 and H3K9me3 signal colocalizing with the GFP signal in wild-type (wt), *met-2*, and *set-25* embryos from *B*. Yellow shading monitors maintenance and violet shading reflects de novo establishment of the marks on offspring from a *met-2 set-25* double mutant. $N = 3$, $n = 68$. (****) $P < 0.00001$ by two-sided Wilcoxon signed-rank test for H3K9me2 *met-2* versus *set-25* following crosses with the *gwIs4 met-2 set-25* parent.

Two relevant characteristics might distinguish these two HMTs: First, they could have distinct targeting mechanisms that restrict the sites they modify, and second, they may have become specialized for either the establishment or the maintenance of their mark. To address this latter, we tested the capacity of SET-25 or MET-2 to establish H3K9me2/me3-marked domains de novo on a well-characterized heterochromatic reporter (*gwIs4*) (Fig. 1B). In N2 worms (wild-type [wt]), this integrated reporter array carries both H3K9me2 and H3K9me3, and contrary to our initial model (Towbin et al. 2012), both HMTs remain bound to the repressed array (Towbin et al. 2012; Delaney et al. 2019). Because the *gwIs4* reporter can be visualized by GFP-LacI, we can monitor the methylation state of the array on a single cell level using immunofluorescence (Supplemental Fig. S1A). By mating reporter-bearing hermaphrodites that are devoid of H3K9me (*met-2 set-25*), with males carrying null alleles of either *met-2* or *set-25,* we could examine the offspring for de novo establishment of H3K9 methylation on the array. Offspring would express SET-25 or MET-2 only, but not both (Fig. 1B).

We first performed a control cross in which the heterochromatic reporter was carried by a silencing-competent N2 hermaphrodite, and therefore had both H3K9me2 and H3K9me3 on the array. In this case, either MET-2 or SET-25 was able to maintain H3K9 methylation over multiple generations (Fig. 1B,C, yellow shading; Supplemental Fig. S1A). We note that in *set-25* offspring H3K9me3 was lost, but the array retained H3K9me2, while in the *met-2* cross H3K9me3 was favored (Fig. 1C). We conclude that either *C. elegans* H3K9 HMT can maintain a H3K9me2- or me3-marked domain over three generations. However, when the reporter array came from a *met-2 set-25* background and thus started in a derepressed, unmethylated state (Towbin et al. 2012), the cross with the *set-25* mutant was unable to generate an H3K9me-marked domain (Fig. 1C, blue shading; Supplemental Fig. S1A), while the *met-2*-deficient worms could. In other words, the establishment de novo of a repressive H3K9me domain required SET-25 (Fig. 1C). This result was surprising, given the more robust role played by MET-2 in the maintenance of repeat methylation (Padeken et al. 2019). Nonetheless, these immunostaining results were verified by ChIP qPCR for H3K9me2 and H3K9me3 using primers specific for the *gfp* gene on the *gwIs4* reporter (Supplemental Fig. S1B). In conclusion, even though SET-25 can be replaced by MET-2 to repress many genomic loci where they work sequentially, the H3K9me3 HMT SET-25 has a unique ability to establish de novo H3K9me-mediated repression.

SET-25 methylates H3K9 preferentially at intact, nondegenerated transposable elements

To understand the relevance of SET-25 mediated repression at endogenous loci, we identified sites where SET-25 confers H3K9me2/me3 in the absence of MET-2 using genome-wide ChIP-seq (Fig. 2A; Padeken et al. 2019). In early stage *met-2* embryos H3K9me2 signal was lost, while ~13.2% of H3K9me3-marked sites were retained in well-bounded peaks (mean domain size ≅3.8 kb in *met-2* vs. 9.7 kb in wt) (Fig. 2A,B). Intriguingly, the absence of H3K9me2 in *met-2* worms argued that SET-25 is very processive, generating almost exclusively H3K9me3, with neither me1 nor me2 intermediates detected (Fig. 2B; Towbin et al. 2012).

The majority of SET-25-dependent H3K9me3 loci (54.4%) mapped to repetitive elements (REs) (Fig. 2C; for wt, see Supplemental Fig. S2C). Among the RE families that were selectively targeted by SET-25 in the absence of MET-2, we found H3K9me3 most enriched on RNA and DNA transposons (listed in Fig. 2D, RE annotation was taken from DFAM.org). A low percentage of three satellite repeats (RC123, RC35, and RC35S) was also detected (Fig. 2D; Supplemental Fig. S2A). Of the MET-2-independent SET-25 targets, 15.5% were silent genes, and 26.4% mapped to intergenic regions, which in some cases colocalize with enhancers (Fig. 2C; Daugherty et al. 2017).

The transposable elements (TE) modified by SET-25 in a MET-2-independent manner did not define one subfamily, but belonged to families that generally retain competence for transposition; that is, TC1-5, MARINCE1 (CemaT1), Mirage1, and Chapaev1-2 families (Bessereau 2006; Hubley et al. 2016; Zeller et al. 2016; Wallis et al. 2019). These are thought to be evolutionarily "young" transposons, meaning that their sequences have not diverged sufficiently to inactivate transposition.

We used the DFAM alignment score, which compares the alignment of a given TE with the repeat consensus sequence, to determine whether SET-25 indeed preferentially targets repeats with a high level of conservation. We plotted the enrichment of H3K9me2 and H3K9me3 on all TEs sorted as high (>5000), medium (<5000 and >1000), or low (<1000) conservation scores (Fig. 2E). TEs with a high conservation score preferentially carried H3K9me3 in both wt and *met-2* mutant embryos, while the MET-2-mediated H3K9me2 on repeats like MSAT1, showed little correlation with the degree of conservation (Fig. 2E,F). The alignment of the copies of the potentially active DNA transposon TC1 and the RNA transposon LINE2A showed strong retention of H3K9me3 across the full transposon even in *met-2* mutants (Fig. 2F), as observed for other intact transposons (Supplemental Fig. S2A,B). This is in contrast to satellite repeats, which lose their H3K9me2 mark upon *met-2* ablation (Fig. 2E, F; Supplemental Fig. S2A,B; Padeken et al. 2019). In conclusion, SET-25 specifically represses highly conserved DNA/RNA transposons independently of MET-2.

Argonaute NRDE-3 and MBT domain protein LIN-61 are essential for SET-25 targeting

Given that SET-25 can establish H3K9me3-containing heterochromatin independently of MET-2, but also trimethylate MET-2-dependent H3K9me2 (Fig. 2A), we suspected that more than one mechanism likely recruits SET-25 to its targets. To identify these factors we again made use of the GFP-tagged heterochromatic reporter,

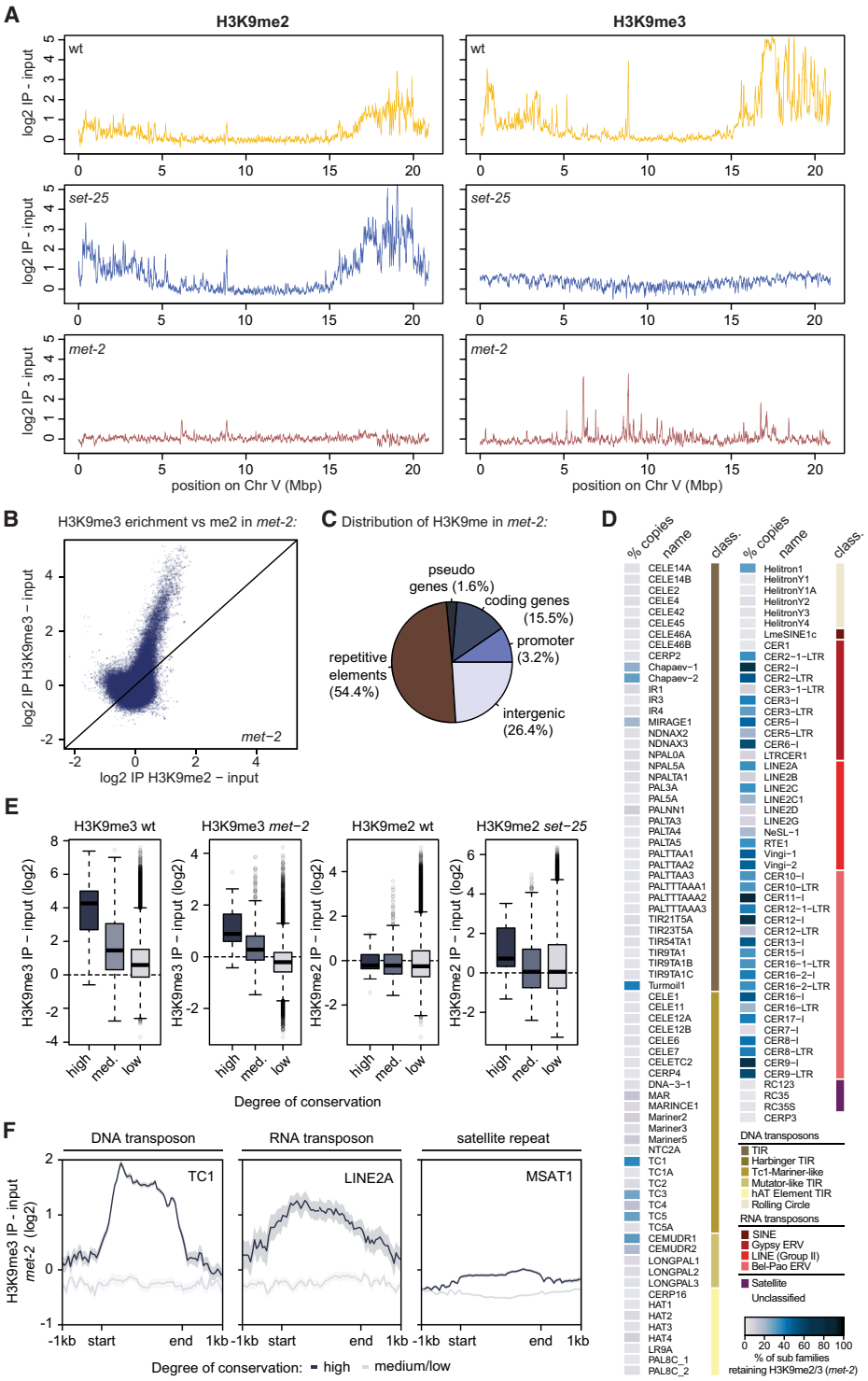

Figure 2. Nondegenerated transposons and a subset of genes retain H3K9me3 in *met-2* mutant. (*A*) H3K9me2 and H3K9me3 ChIP-seq was performed on early embryos (up to 100 cells) at 20°C in wt, *set-25*, and *met-2* strains. The mean $\log_2$ enrichment over input along a typical autosome, Chr V, is shown ($N = 2$). (*B*) Scatter plot correlating the genome-wide mean $\log_2$ fold change of H3K9me3 over input to the mean $\log_2$ fold change of H3K9me2 over input at 500-bp intervals in the *met-2* mutant. (*C*) Percentage of H3K9me2- or me3-positive loci (log2 IP over input >1) overlapping with pseudo genes, genes, repetitive elements, and intergenic regions in *met-2* mutant embryos. (*D*) Percentage of repetitive element copies per repeat subfamily (DFAM annotation) that retain H3K9me2/me3 in *met-2(n4256)* mutants at minimum two copies per subfamily. Repeat classification (class.) is annotated by color code at the *left*. (*E*) The mean enrichment of H3K9me3 and H3K9me2 IP over input at repetitive elements with a high (>5000), medium (<5000 and >1000), or low (<1000) conservation score (based on DFAM bit score) in wt, *met-2*, and *set-25* mutants. (*F*) Metaplots of mean $\log_2$ fold change H3K9me3 over input in the *met-2* mutant at TC1 (Tc1-Mariner-like DNA transposon), LINE2A (LINE [class II] RNA transposon) and MSAT1 (satellite repeat) repetitive elements with a high conservation score (dark blue) and medium/low conservation score (gray). H3K9me3 in *met-2* mutant cells is enriched only on conserved elements. Standard deviation between individual regions is indicated as a semitransparent shading.

and monitored colocalization with a mCherry-tagged SET-25 (mCh::SET-25) in both wt and *met-2* mutant embryos (Fig. 3A,B; Towbin et al. 2012). Using RNAi, we down-regulated the expression of 52 candidate factors, all of which had been previously identified as essential for the silencing of heterochromatic arrays and/or of a TC1 reporter (Vastenhouw et al. 2003; Grishok et al. 2005; Towbin et al. 2012). Scoring for the nuclear dispersion of mCh::SET-25 following RNAi, we found four genes, *nrde-2*, *nrde-3*, *nrde-4*, and *lin-61*, to be necessary for the colocalization of mCh::SET-25 with the GFP-marked foci (Fig. 3C–F; Supplemental Fig. S3A). RNAi against *lin-61,* a known H3K9me reader that binds all three H3K9me states (Koester-Eiserfunke and Fischle 2011), triggered the release of SET-25 in both wt and *met-2* backgrounds. In contrast, knockdown of *nrde-2, nrde-3,* and *nrde-4* interfered with SET-25 localization only in the absence of MET-2 (Fig. 3C,F). This suggests that the NRDE pathway acts in parallel to a recruitment pathway that depends on MET-2.

NRDE-3 is a somatic Argonaute that has been shown to be essential for the silencing of targets of exogenous dsRNA (Guang et al. 2008, 2010; Gent et al. 2010). The conserved NRDE-2, as well as NRDE-4, are essential for NRDE-3 mediated silencing (Guang et al. 2010; Burkhart et al. 2011; Burton et al. 2011). ERGO-1, an Argonaute that acts upstream of NRDE-3 and other small RNA pathways (Gent et al. 2010; Montgomery et al. 2012; Almeida et al. 2019a), showed a partial loss of SET-25 localization (Fig. 3C–F), consistent with either a partial knockdown by *ergo-1* RNAi, or a maternal contribution of *ergo-1* or ERGO-1-dependent small RNAs (Almeida et al. 2019b). Growing the worms on the RNAi (*ergo-1)* for two generations was impossible due to the high level of germline sterility that stems from *ergo-1* knockdown in the *met-2* deficient background. In any case, NRDE-3 is the central and best characterized Argonaute in this siRNA pathway (Fig. 3D), and its down-regulation showed the most robust loss of SET-25 localization to the heterochromatin array. We therefore focused on the role of the NRDE-3 Argonaute in SET-25 targeting.

Importantly, we note that the loss of transcriptional silencing alone is not sufficient to release SET-25 from the array. RNAi of the heterochromatin protein 1 (HP1) homologs *hpl-1* and *hpl-2* or the Polycomb proteins *mes-2* (EZH2) and *mes-6* (EED) homologs were similarly tested in the RNAi screen, and all triggered transcriptional derepression of the reporter without interfering in SET-25 colocalization to this array (Fig. 3C,F; Towbin et al. 2012; Mattout et al. 2020).

LIN-61 is required for SET-25 targeting, H3K9me3 levels, and transcriptional repression

In *set-25* mutants we detected robust levels of H3K9me2 at many sites that had carried H3K9me3 in wt embryos (Fig. 2A; Padeken et al. 2019). In other words, MET-2-deposited H3K9me2 can both replace SET-25's mark, and serve as the substrate for SET-25-mediated trimethylation. In cases in which SET-25 is recruited to MET-2-dependent H3K9me2, a molecular bridge is needed to link the modified histone tail to SET-25, as this HMT has no methyl-lysine binding capacity. Conveniently, the second factor identified in our screen, LIN-61, is indeed required for SET-25 targeting to the array (Fig. 3C–F), and appears to serve this role as mediator thanks to its four MBT domains that bind H3K9me1, me2, or me3 (Koester-Eiserfunke and Fischle 2011). The *lin-61* RNAi in embryos expressing fluorescent SET-25, led to a loss of endogenous SET-25 foci (Fig. 4A,B), yet it did not alter the presence of MET-2 foci (Delaney et al. 2019). This is consistent with MET-2 being upstream of LIN-61, and independent of either SET-25 or LIN-61 recruitment. It also predicts that the loss of *lin-61* should compromise H3K9me3.

To confirm this, we characterized changes in H3K9me2 or H3K9me3 in a *lin-61*-null allele (Fig. 4C–D). Absolute values for H3K9me2 and H3K9me3 immunofluorescence in the *lin-61* mutant revealed a strong reduction in H3K9me3 to roughly the same level found in *met-2*-null strains [mean fold reduction (*lin-61*) = 2.4 vs. (*met-2*) = 2.5] (Fig. 4D). Moreover, in compensation, we note a mean 1.4-fold increase in H3K9me2 ($P < 2 \times 10^{16}$) in the *lin-61* mutant (Fig. 4D). Interestingly, the *lin-61;met-2* double mutant showed an additional drop in H3K9me3 [mean fold reduction (*lin-61;met-2*) = 4.8] (Fig. 4D), arguing that LIN-61 promotes SET-25 activity even on the NRDE-3 pathway, which is independent of MET-2. The overall level of histones does not drop significantly in any of the mutants tested in this assay (Supplemental Fig. S1C,D). Thus, we envision that LIN-61 could be an allosteric enhancer of SET-25 catalytic activity, as well as a bridge from H3K9me2 to the enzyme. Whether it acts alone or in a complex is unclear.

To identify the sites at which LIN-61 mediates SET-25 activity, we compared H3K9me3 ChIP-seq in wt, *lin-61*, and *met-2* embryos (Fig. 4E–G). Comparing the distribution and intensity of the H3K9me3 mark, we found that in all combinations (wt vs. *lin-61,* or *met-2* vs. *lin-61; met-2* double), the loss of *lin-61* led to a general reduction at all H3K9me3-marked sites, affecting the signal level across the entire methylated gene or domain (Fig. 4E,F; Supplemental Fig. S3B). We note that neither the efficiency of spreading nor the boundaries of H3K9me3 domains changed upon loss of LIN-61, but rather the trimethyl abundance or "intensity" was reduced (Fig. 4G; Supplemental Fig. S3B). This was true for sites that are MET-2-dependent, as well as those that are MET-2-independent targets.

We next correlated the reduction of H3K9me3 levels observed in the *lin-61* mutant with the efficiency of transcriptional silencing. We performed total RNA-seq in early embryos isolated from *lin-61*, *met-2*, and *set-25* single mutants, followed by studies of double alleles. Loss of *lin-61* led to the up-regulation of 332 genes (FDR < 0.01 and $\log_2$ FC > 2) (Fig. 5A) and 104 individual copies of repetitive elements (FDR < 0.05 and FC > 2) (Fig. 5A). We ruled out that *set-25* expression itself was reduced upon loss of *lin-61* and showed that histone levels also do not change significantly (Supplemental Fig. S4B). We found that the loci derepressed in *lin-61* are indeed among those

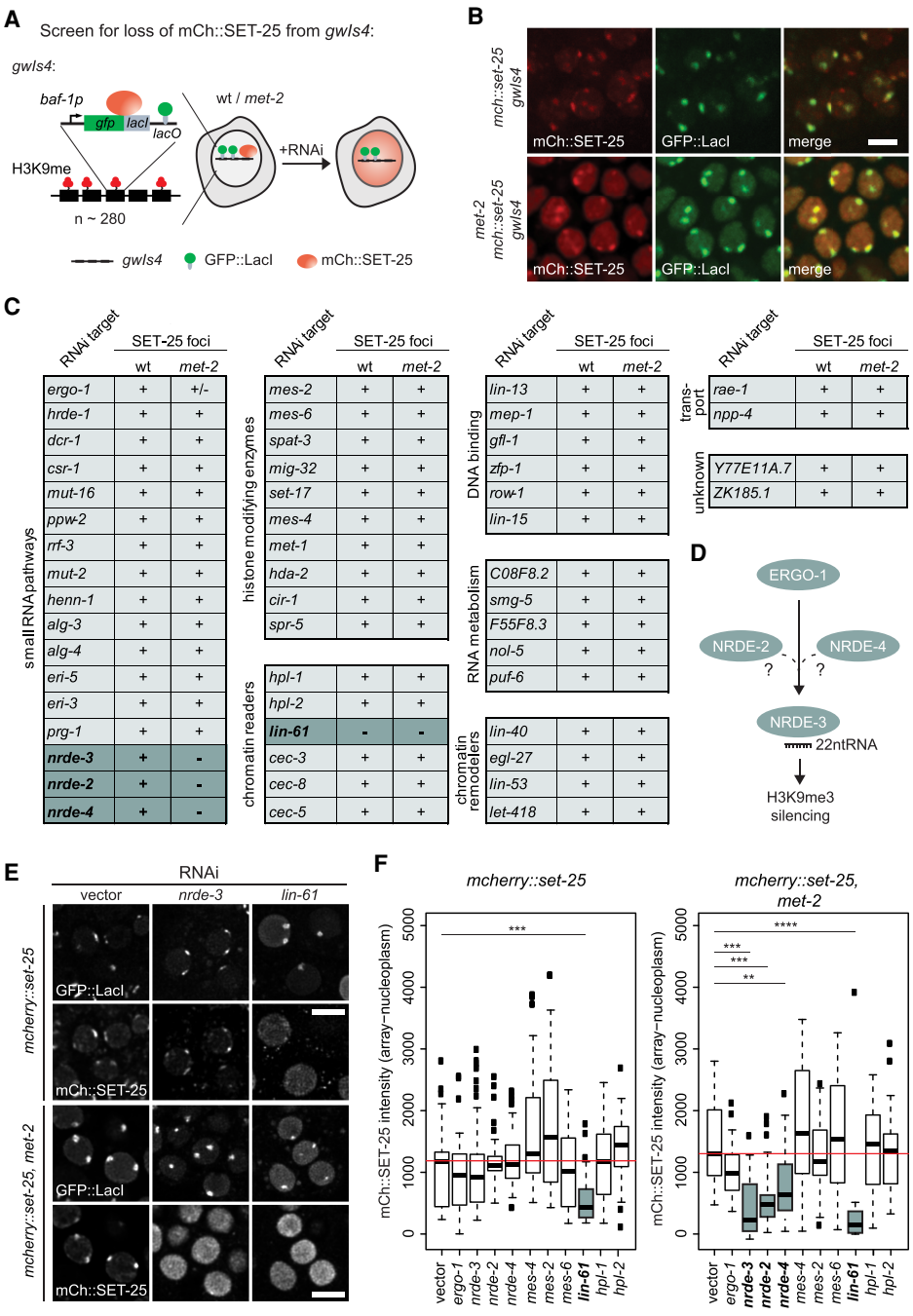

Figure 3. RNAi screen identifies Argonaut NRDE-3 and MBT domain protein LIN-61 as essential for SET-25 targeting to heterochromatin. (*A*) Scheme describing the RNAi screen for factors essential for SET-25 targeting to the heterochromatic reporter (*gwIs4*). Wild-type (wt) and *met-2* mutant worms expressing *gfp::lacI* from the heterochromatic reporter (*gwIs4*) were treated with RNAi against candidate genes, or empty vector (L4440). F1 embryos were screened for loss of colocalization of the mCherry::SET-25 and GFP::LacI. (*B*) Live-cell fluorescent images of wt and *met-2(n4256)* embryos, ectopically expressing *mcherry::set-25* and *gfp::laci* from the *gwIs4* heterochromatic reporter (Towbin et al. 2012) showing colocalization. Scale bar, 5 µm. (*C*) Table summarizing the 52 RNAi candidate screen. Effect of knockdown on mCherry::SET-25 foci in wt and *met-2* mutants are indicated next to the gene name. (+) Foci present, (+/−) foci absent in a subset of embryos, (−) no foci present. Hits that showed no foci are highlighted in a darker gray. Candidates are grouped according to biological function (source http://www.wormbase.org). $N = 3$, nuclei scored per RNAi event = 25. (*D*) Scheme of siRNA pathway from ERGO-1, NRDE-2/-3/-4, to transcriptional (trx.) silencing and H3K9me3 in the somatic small RNA pathway. Dotted lines indicate genetic links, solid lines reflect molecular evidence, and "?" indicates putative mechanisms. (*E*) Live-cell images of embryos expressing *mcherry::set-25* and *gfp::lacI* from the *gwIs4* heterochromatic reporter in wt and *met-2* embryos treated with RNAi against *lin-61* and *nrde-3* or the vector control. Scale bar, 5µm. (*F*) Quantitation of mean fluorescence signal intensity from mCherry::SET-25 at the GFP::LacI foci normalized to mean mCherry::SET-25 signal in the nucleoplasm, from selected RNAi knockdowns in wt and *met-2* embryos, ruling out roles for Polycomb (*mes-2* and *mes-6*) and HP1 homologs (*hpl-1* and *hpl-2*). RNAi targets resulting in a significant reduction of the mCherry::SET-25 enrichment on the *gwIs4* array are shaded in gray. *P*-values were calculated using one-sided Anova and are indicated *above* box plots. (****) $P < 0.00001$; (***) $P < 0.0001$; (**) $P < 0.001$. $N = 3$, $n = 25$.

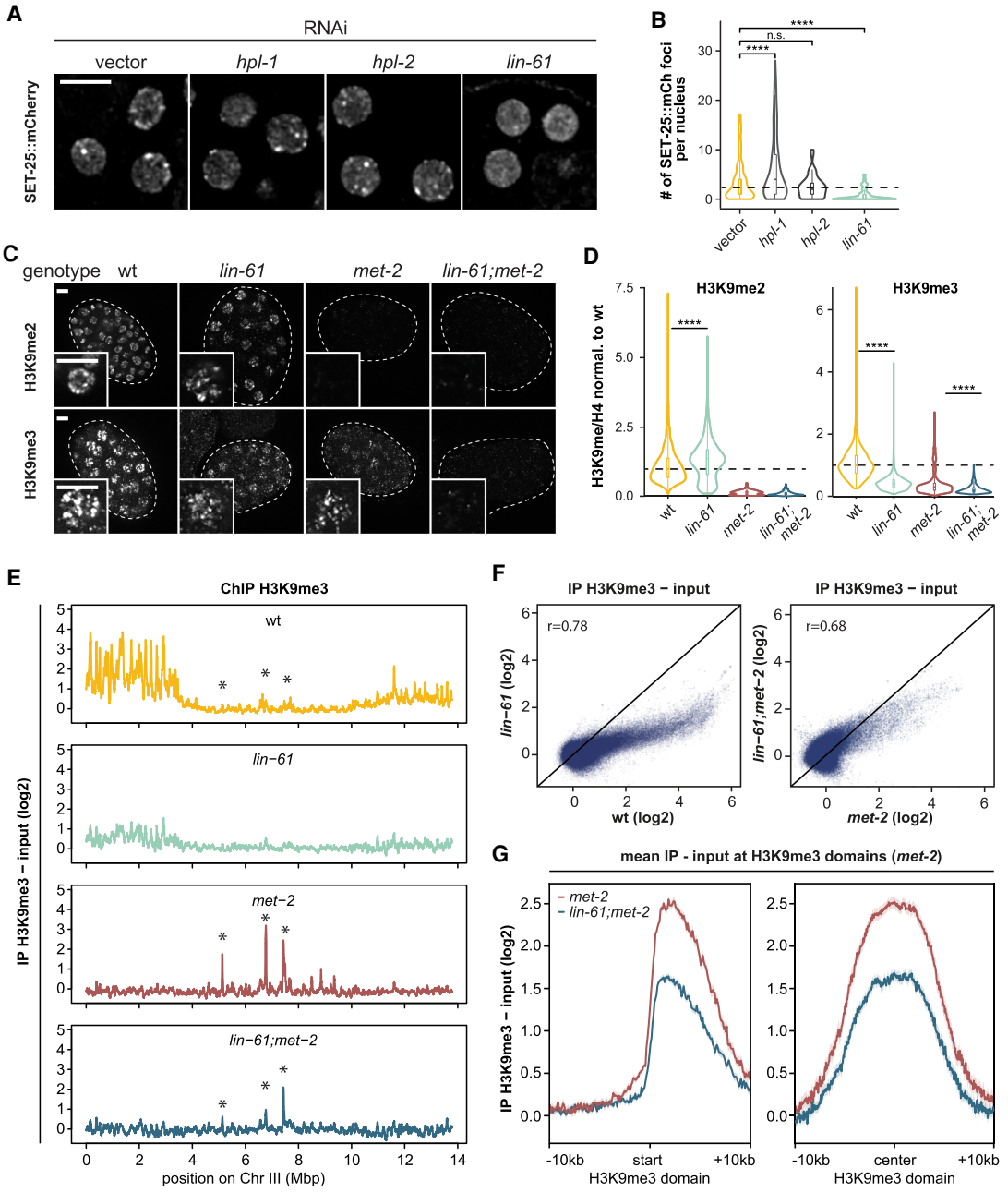

Figure 4. RNAi or deletion of *lin-61* results in a loss of SET-25 targeting and a reduction in H3K9me3. (*A*) Live cell imaging of foci of endogenously tagged SET-25::FLAG::mCherry (SET-25::mCherry) upon RNAi of the HP1 homologs *hpl-1* and *hpl-2* and the MBT domain protein *lin-61*. Synchronized L1 were exposed to RNAi and embryos of the F1 generation were imaged. A typical nucleus for each is enlarged. Scale bar, 5 µm. (*B*) Quantitation of SET-25::mCherry foci number per nucleus in the embryos shown in panel *A* using automated image analysis. $N = 2$, n(vector):236, n(*hpl-1*):445, n(*hpl-2*):288, n(*lin-61*):308. *P*-values were calculated using two-sided ANOVA and are indicated *above* violin plots. (****) *P*-value<0.00001; (n.s.) not significant). (*C*) H3K9me2 and H3K9me3 immunostaining of embryos isolated from wild-type (wt), *met-2, lin-61(tm2649)* (hereafter labeled *lin-61*), and *lin-61(tm2649);met-2* mutants. Scale bar, 5 µm. (*D*) Mean immunofluorescence signal of H3K9me2 and H3K9me3 normalized to H4 using automated image analysis. For H3K9me2, $N = 2$; wt $n =$ 1917, *met-2* $n = 1088$, *lin-61* $n = 1147$, *lin-61;met-2* $n = 1027$. For H3K9me3, $N = 3$; wt $n = 1467$, *met-2* $n = 851$, *lin-61* $n = 2455$, *lin-61;met-2* $n = 1813$. *P*-values were calculated using a two sided ANOVA; H3K9me3: *P*(wt vs. *lin-61*) < 0.00001, *P*(*met-2* vs. *lin-61;met-2*) < 0.00001. (*E*) H3K9me3 ChIP-seq was performed on early embryos at 20°C in wild-type (wt), *met-2, lin-61*, and *lin-61;met-2* strains. The mean $\log_2$ enrichment over input along a typical autosome, Chr III, is shown ($N = 3$). Asterisks mark regions that show H3K9me3 in *met-2* and a reduction in *lin-61;met-2*. (*F*) Scatter plot showing the correlation of the genome-wide H3K9me3 enrichment over input ($\log_2$) counted >500-bp bins in wt and *lin-61*, as well as *met-2* and *lin-61;met-2* mutants. *r* = Pearson correlation coefficients for both correlations. (*G*) Metaplots compare mean enrichment of H3K9me3 over input in domains retained in either *met-2* single (red) or *lin-61;met-2* double (blue) mutants. Plots are anchored at the start (*right* panel) or the center (*left* panel) of the domains. See Supplemental Figure S4A for H3K9me3 signal at individual domains.

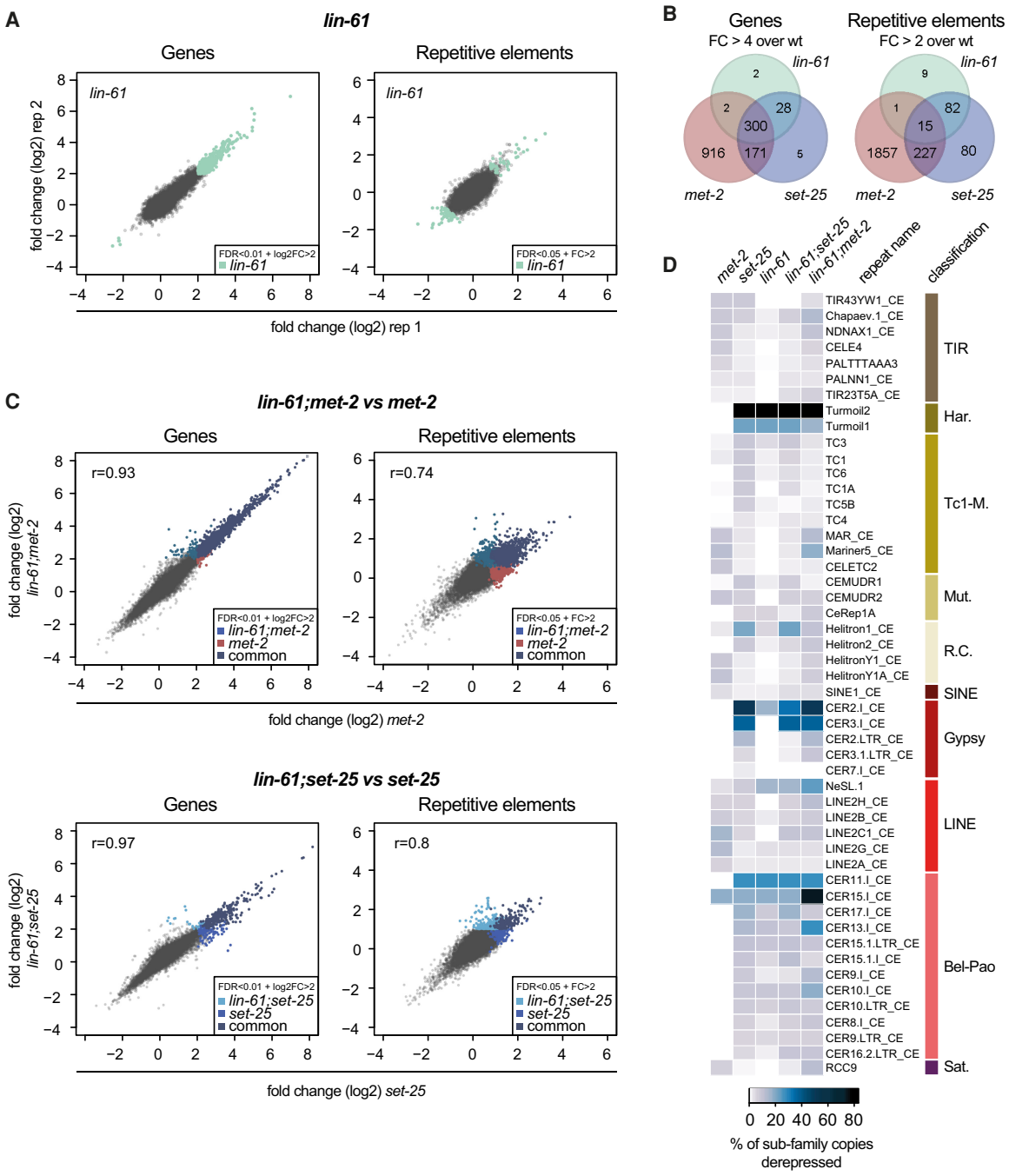

Figure 5. Loss of *lin-61* is epistatic with *set-25* for the derepression of genes and repetitive elements. (*A*) Scatter plot of transcripts from genes as $\log_2$ fold change over wt in early embryos of *lin-61* mutants (two replicas shown, $N = 3$) at genes (*left* column) and from repetitive elements (*right* column). Loci significantly changed are in cyan (genes: FDR 0.01 and $\log_2$ fold change >2 or <−2; repetitive elements: FDR 0.05 and fold change >2 or <−2). (*B*) Venn diagrams showing the overlap between genes and repetitive elements derepressed in *lin-61*, *met-2*, and *set-25* single mutants (genes: FDR 0.01 and $\log_2$ fold change >2 or <−2; repetitive elements: FDR 0.05; and fold change >2 or <−2). (*C*) Correlation between the fold change ($\log_2$) over wt for gene and repetitive element transcripts between *met-2* or *set-25* single and *lin-61; met-2* and *lin-61;set-25* double mutants. Loci significantly changed compared with wt (genes: FDR 0.01 and $\log_2$ fold change >2 or <−2; repetitive elements: FDR 0.05; and fold change >2 or <−2) are colored according to the genotype and loci significantly changed in both of the two compared genotypes are colored in dark purple. Pearson correlation coefficients (*r*) are in figures. (*D*) Percentage of derepressed copies per repeat subfamily of the 50 most derepressed repeat subfamilies from *set-25*, analyzed *in met-2, set-25, lin-61, lin-61;set-25,* and *lin-61;met-2* mutants, as indicated. Repeat name and classification according to DFAM are indicated next to heat map. (TIR) Terminally inverted repeat, (Har.) harbinger TIR DNA transposon, (Tc1-M.) Tc1-Mariner-like DNA transposon, (R.C.) rolling circle DNA transposon, (SINE) short interspersed nuclear elements, (Gypsy) Gypsy endogenous retrovirus, (LINE) long interspersed nuclear elements (class II), (Bel-Pao) Bel-Pao endogenous retrovirus, (Sat.) satellite repeat.

derepressed in the single HMT mutants, that is, those affected by the loss of either *met-2* or *set-25* (Fig. 5B; Supplemental Fig. S4A,C). Importantly, basically all genes derepressed by loss of *lin-61* were derepressed by the loss of *set-25* (98.8%) (Fig. 5B; Supplemental Fig. S4C). Since MET-2 is necessary for SET-25 targeting to most genes (Zeller et al. 2016; Padeken et al. 2019), we also scored an extensive overlap between *met-2*- and *lin-61*-sensitive loci. Nonetheless, we note that not all *set-25*-sensitive genes are derepressed by the loss of *lin-61*, suggesting that at some loci the partial drop in H3K9me3 observed in the *lin-61* mutant still can repress transcription (e.g., Fig. 4G).

The repeat elements that one might expect LIN-61 to control are those that bear H3K9me3, which defines a subset of RNA and DNA transposons (Padeken et al. 2019). Indeed, the top 50 repeat subfamilies derepressed in the *set-25* mutant are DNA and RNA transposons (Fig. 5D), and those derepressed by *lin-61* ablation are indeed a subset of the H3K9me3-marked transposons up-regulated in the *set-25* mutant (Fig. 5C; Supplemental Fig. S4D). Thus, LIN-61 affects a subset of SET-25-regulated REs and genes, and *set-25* has a stronger impact than *lin-61* on repression.

To confirm the epistatic relationship of LIN-61 and the two HMTs, we analyzed double mutants. We found almost complete correlation among genes derepressed in the *set-25* single and the *lin-61;set-25* double mutant (genes: Pearson $r = 0.97$) (Fig. 5C) and only slightly less correlation for REs (Pearson $r = 0.8$). The correlation between the *met-2* single and *lin-61;met-2* double was only slightly weaker (genes: Pearson $r = 0.93$; REs: Pearson $r = 0.74$) (Fig. 5C). In other words, *lin-61* effects are indeed epistatic with respect to SET-25 targets: LIN-61 enhances the SET-25 activity both at MET-2-independent sites and at MET-2-sensitive sites, where LIN-61 appears to enhance SET-25 recruitment to H3K9me2.

The Argonaute NRDE-3 and 22G RNAs are required for MET-2-independent SET-25 localization

In contrast to the loss of LIN-61, which impaired SET-25 recruitment both in the presence or absence of MET-2, we only scored SET-25 mislocalization after *nrde-3* RNAi in the absence of MET-2 (Fig. 3). This suggests that the role played by NRDE-3 in targeting of SET-25 is likely to be masked, or substituted for, by the presence of MET-2. NRDE-3 has been shown to bind and silence through small RNAs and H3K9 methylation (Guang et al. 2008). To confirm that *nrde-3* targets SET-25 to endogenous sites of action in the absence of MET-2, we analyzed endogenous SET-25::mCherry foci in wt, *met-2*, *nrde-3* worms, and the *met-2;nrde-3* double mutant (Fig. 6A). While loss of *met-2* resulted in a partial delocalization of SET-25::mCherry foci, the *nrde-3* single mutant led to no pronounced change in SET-25 localization, just as we had observed with the *gwIs4* array. However, *met-2;nrde-3* double mutant led to the complete dispersal of SET-25 signal (Fig. 6A). Moreover, as expected, *nrde-3* loss had no effect on endogenous MET-2 foci (Supplemental Fig. S5B). This shows clearly that NRDE-3 is responsible for targeting SET-25 to heterochromatic foci in the absence of MET-2.

The Argonaute NRDE-3 preferentially binds small RNAs that are 22 nucleotides long (22 nt called 22G here) in somatic cells (Gu et al. 2009). If NRDE-3 recruits SET-25 to sites of repression through its RNA binding ability, then one might expect to detect small RNAs mapping to the regions that retain H3K9me3 in *met-2* mutants (Batista et al. 2008; Bonasio et al. 2010). Indeed, small RNA sequencing showed that 22G RNAs were enriched at sites that retain H3K9me3 in *met-2* mutants (*met-2*-independent domains) (Fig. 6B), but were not enriched at sites where H3K9me3 was dependent on MET-2 (*met-2*-dependent domains) (Fig. 6B). In addition, we mapped 22G RNAs to the *gwIs4* heterochromatic reporter (Supplemental Fig. S5A). Interestingly, while loss of *met-2* induces the transcriptional up-regulation of the reporter (Towbin et al. 2012), we only saw a minor up-regulation of its 22G RNAs in *met-2* mutants (Supplemental Fig. S5A), arguing that transcription is not sufficient for the production of small RNAs. Interestingly, while 22G RNAs map only to the negative strand of the *gwIs4* reporter, as expected (Pak and Fire 2007; Sijen et al. 2007; Gu et al. 2012), the transposon-enriched *met-2*-independent H3K9me3 regions showed 22G RNA enrichment on both DNA strands. We can explain their presence on both positive and negative strands because most of these full-length transposons have RNA Pol II promoters driving transcription on both strands (Feuchter and Mager 1990; Domansky et al. 2000; Dunn et al. 2006; Yang and Kazazian 2006). Indeed, we found 22G RNAs on both strands of the TC1 transposable element as well (Supplemental Fig. S5D; Raizada et al. 2001; Palazzo et al. 2019). The 22G RNA levels did not change in the absence of *met-2,* but dropped over target genes in the *nrde-3* mutant (Fig. 6B; Supplemental Fig. S5C), mimicking the behavior of 21U RNAs at target sequences of the Piwi Argonaute in *prg-1* mutants (Batista et al. 2008). The fact that the 22G RNAs are independent of MET-2 shows clearly that this HMT is not important for the Argonaute-SET25 targeting pathway. Indeed, the *nrde-3*-dependent accumulation of 22G RNAs occurs on TC1 transposons that retain H3K9me3 in *met-2* mutants (Fig. 2F; Supplemental Fig. S5D). We confirmed that no small RNAs arise from transposons that do not retain H3K9me3 in *met-2* mutants. Moreover, by RIP-qPCR (UV-crosslinked RNA immunoprecipitation) NRDE-3 is shown to bind RNA originating from transposable elements, but not from satellite sequences or single-copy genes (Supplemental Fig. S5E). Taken together, our findings indicate that NRDE-3 recruits SET-25 independently of MET-2, through an association with small RNAs generated from the bidirectional transcripts of transposable elements.

We next asked whether the loss of *nrde-3* alters H3K9me2/me3 levels either globally or at specific loci. This is particularly important to establish, because the *lin-61* mutant had a global or general effect on all SET-25 targets. First, by comparing total H3K9me2/me3 levels by immunostaining of embryos of wt versus *nrde-3* or

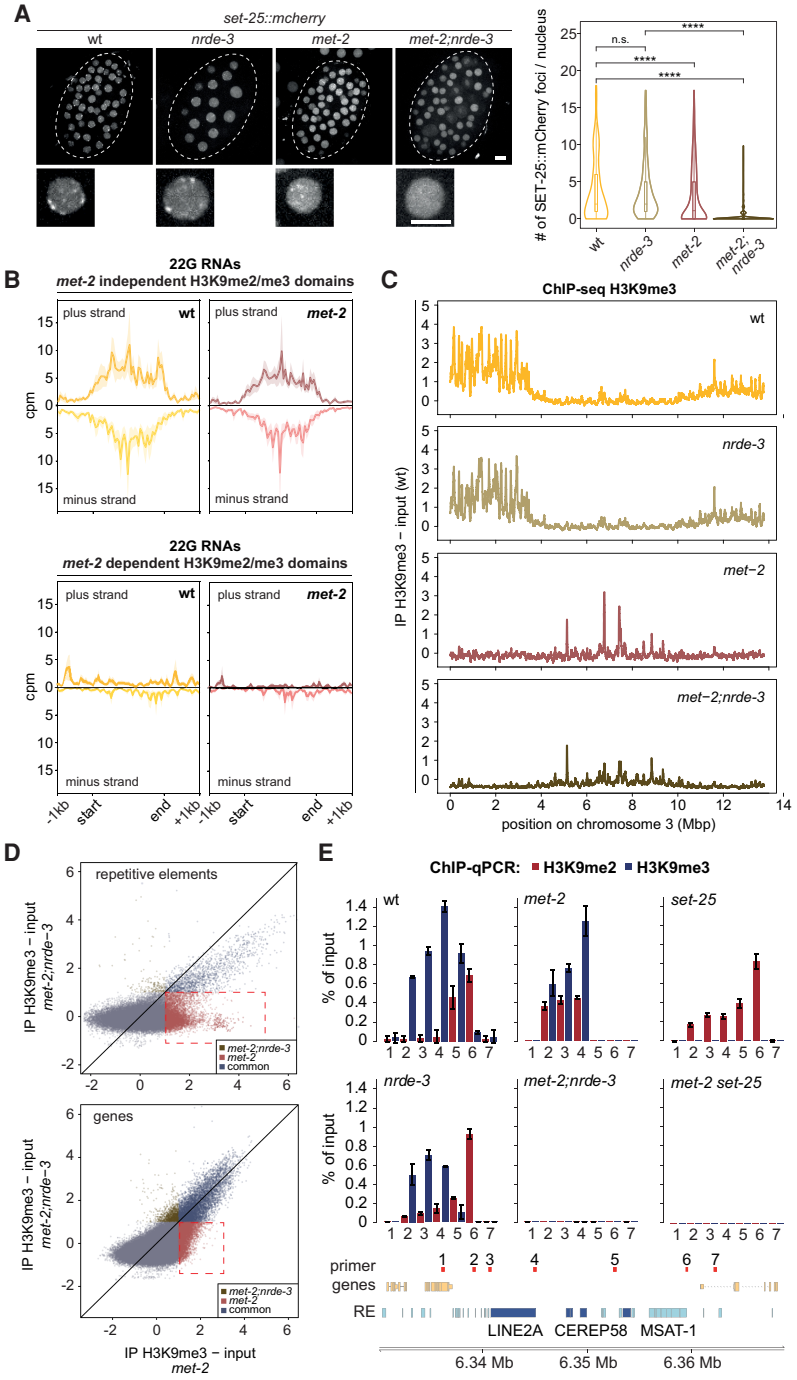

Figure 6. NRDE-3 targets SET-25 to conserved DNA and RNA transposons in a manner that is parallel to and independent of MET-2. (*A*) Live-cell imaging and quantitation of endogenous *set-25* fused to *flag::mcherry* (*set-25::mcherry*) in wt, *nrde-3 (tm1116)* (hereafter *nrde-3*), *met-2*, and *met-2; nrde-3(tm1116)* mutant embryos. Scale bar, 5 µm. Quantitation of SET-25::mCherry foci per nucleus using automated image analysis. $N = 3$, n(wt):540, n(*met-2*):769, n(*nrde-3*):590, n(*met-2;nrde-3*):1020 ; *P*-values were calculated using two-sided ANOVA and are indicated *above* violin plots. (****) *P*-value < 0.00001, (n.s.) not significant. (*B*). Mean counts of 22-nt RNA in counts per million (cpm) in wt and *met-2* (for *nrde-3 and met-2;nrde-3*) (see Supplemental Fig. S6C) early embryos over domains that either retain H3K9me3 in *met-2* mutants (*met-2*-independent), or lose H3K9me3 in a *met-2* mutant, but retain/gain H3K9me2 in *set-25* (met-2-dependent), split byDNA strand. Solid lines indicate the mean signal and shaded regions the standard deviation. (*C*) H3K9me3 ChIP-seq performed on early embryos at 20°C in wt, *nrde-3, met-2,* and *met-2;nrde-3* strains. Mean $\log_2$ enrichment over input along a typical autosome, Chr III, is shown ($N = 2$). (*D*) Scatter plot correlating the H3K9me3 signal over input ($\log_2$) in *met-2;nrde-3 met*-double mutants with *met-2* single mutants at repetitive elements and genes. Red indicates loci enriched for H3K9me3 in *met-2*, but not in *met-2; nrde-3* ($\log_2$ fold change >1 in *met-2* and <1 in *met-2;nrde-3*). These are marked with a red rectangle. Colored in dark purple are loci common to both genotypes ($\log_2$ fold change >1 in *met-2* and >1 in *met-2;nrde-3* and genes exclusively H3K9 trimethylated in *met-met-2;nrde-3* are colored in brown. (*E*) ChIP qPCR of H3K9me2 and H3K9me3 in wt, *met-2*, *set-25(n5021)* (hereafter *set-25*), *nrde-3*, *met-2;nrde-3*, *met-2 set-25*, and *set-25;nrde-3* mutant embryos using primers spanning a domain on Chr III that retains H3K9me3 in *met-2* mutants ($N = 3$; bars indicate mean, error bars indicate SD) (for control loci, see Supplemental Figs. S2A, S6E).

met-2 versus *met-2;nrde-3* mutants, we found no global change in H3K9me2/me3 levels upon loss of NRDE-3 (Supplemental Fig. S6A). Because this was surprising, we used ChIP-seq to map the genome-wide distributions of H3K9me3 in wt, *nrde-3*, *met-2,* and *met-2;nrde-3* mutants. Whereas H3K9me3 levels on genes and REs did not change between *nrde-3* and wt strains (Fig. 6C; Supplemental Fig. S6B), we found a strong effect in the *met-2;nrde-3* double mutant versus *met-2* alone. This revealed the strong redundancy between MET-2-dependent and MET-2-independent pathways: The *nrde-3* effect on H3K9me3 was only visible in the absence of MET-2. Remarkably, however, ~67% of all repetitive elements that had retained H3K9me3 in the *met-2* single mutant, lost H3K9me3 in the *met-2;nrde-3* double mutant (Fig. 6D, labeled red, boxed). It is also noteworthy that this was true for REs, but not for genes that were targeted independently of MET-2; genes retained H3K9me3 in the *met-2;nrde-3* double mutant (Fig. 6D, dotted box).

To confirm that the loss of H3K9me3 from SET-25-targeted REs occurred specifically in the *met-2;nrde-3* double mutant, we performed H3K9me2 and H3K9me3 ChIP-

qPCR for two regions at which SET-25 acts independently of MET-2 (Fig. 6E; Supplemental Figs. S2A, S6C). Whereas both H3K9me2 (Fig. 6E, red) and H3K9me3 (Fig. 6E, blue) remained detectable in *met-2* and *nrde-3* single mutants, both marks were completely lost in the *met-2;nrde-3* double mutant (Fig. 6E; Supplemental Fig. S6C). Control genes with no H3K9me remained unmethylated in all cases (Supplemental Fig. S6D). Taken together, our data argue that NRDE-3 targets SET-25 to a subset of transposable elements in a manner that is independent of MET-2 and can only be appreciated in the absence of *met-2*. In other words, NRDE-3-mediated SET-25 targeting is masked by MET-2-dependent H3K9 methylation.

In *S. pombe*, stable siRNA-induced silencing of heterochromatin is reinforced by a feedback loop between the RNA-induced transcriptional silencing complex (RITS; consisting of Ago1, Chp1, and Tas3) and H3K9me2/me3 (Motamedi et al. 2004; Sugiyama et al. 2005). To test whether loss of SET-25, or H3K9me3 impacts the function of NRDE-3 we quantified its nuclear and cytoplasmic abundance by live cell microscopy. Cytoplasmic accumulation of NRDE-3 can be used as a proxy for its function, because its nuclear localization was previously shown to depend on either the abundance of small RNAs or its ability to bind small RNAs through its PAZ domain (Guang et al. 2008). Upon RNAi of *set-25*, but not *met-2* or the empty vector control, we observed only a 10.3% increase in cytoplasmic NRDE-3 (Supplemental Fig. S6E), arguing that the vast majority of NRDE-3 remains functional and nuclear without H3K9me3.

Loss of nrde-3 *and* met-2 *results in the synergistic derepression of transposons*

Once again, it was important to test whether the effects we observed on H3K9 methylation also result in the loss of transcriptional silencing. We performed genome-wide RNA-seq on wt, *met-2*, *set-25*, and *nrde-3* single mutants, as well as the double mutants *met-2;nrde-3* and *set-25; nrde-3*, to see whether NRDE-3 and MET-2 indeed redundantly silence repeats or genes (Fig. 7A,B; Supplemental Fig. S4A). When correlating replicates of transcriptional changes in single mutants over wt, we saw that *met-2* loss has the strongest effect, with 1389 genes and 2211 individual RE copies up-regulated (genes: FDR < 0.01, $\log_2$ fold change >2; RE: FDR < 0.05, fold change >2) (Supplemental Fig. S4A). The *set-25* deletion also resulted in the up-regulation of 504 genes and 404 repeats (genes: FDR < 0.01, $\log_2$ fold change >2; RE: FDR < 0.05, fold change >2) (Supplemental Fig. S4A), while the loss of *nrde-3* alone altered the expression of only 23 genes (16 up, and seven down; FDR < 0.01; $\log_2$ fold change >2 or <−2) (Fig. 7A) and 66 REs (FDR < 0.05; fold change >2 or <−2) (Fig. 7A, gold spots), including the up-regulation of DNA and RNA transposons (Supplemental Fig. S7A,C,E).

Again, the examination of the transcriptomes in double mutants allowed us to determine the epistatic relationships of these factors. Comparison of the *set-25; nrde-3* double mutant with the *set-25* single mutant showed a very high correlation [Pearson r(genes) = 0.94; Pearson r(RE) = 0.78] (Fig. 7B), although 29 genes and 52 RE were additionally up-regulated in the *set-25;nrde-3* double versus the *set-25* single mutant (confirmed by RT-qPCR) (Supplemental Fig. S7B). This largely epistatic relationship is in contrast to the synergistic derepression observed when we compared the *met-2;nrde-3* double mutant versus *met-2* alone (Fig. 7B). Three-thousand-forty repetitive elements were derepressed (boxed) in the *met-2;nrde-3* animals, with an average up-regulation of threefold (compared with mean fold change of 1.8 in the *met-2* single mutant). Notably, 1299 REs were derepressed by ablation of both *nrde-3* and *met-2*, that were not affected by *met-2* or *nrde-3* alone, confirming redundancy between these silencing pathways (Fig. 7B; Supplemental Fig. S7A–C,E).

An analysis of the top 50 derepressed repeat subfamilies in the *met-2;nrde-3* double mutant identified mostly Gypsy and Bel-Pao endogenous retrotransposons (ERVs) and LINE elements (group II) (Supplemental Fig. S7A), but synergistic derepression spanned all types of transposons and affected 40%–80% of the copies within a single repeat class (Supplemental Fig. S7A,E). We confirmed the selectivity and specificity of this *met-2;nrde-3* synergy by qPCR for specific DNA and RNA transposons in single and double mutant backgrounds (Supplemental Fig. S7C). Again, the level of derepression in the *met-2; nrde-3* mutant exceeded that of the *met-2*, *set-25*, and *set-25; nrde-2* doubles, and identified sites that were not derepressed at all in *met-2* or *nrde-3* single mutants.

To see whether NRDE-3 has a preference among transposons, we measured the conservation score of transposons up-regulated by the loss of either *set-25, met-2* or *nrde-3*. Elements with a high conservation score that retain transposition capacity were modestly derepressed in *set-25* (mean $\log_2$ fold change = 0.6) (Supplemental Fig. S7D) and unaffected by *met-2* or *nrde-3* single mutants (Fig. 7C). Interestingly, in the *met-2; nrde-3* double there was an even stronger bias for young TEs among the derepressed repeats (mean $\log_2$ fold change = 1.2) (Fig. 7C). This argues that *met-2* and *nrde-3* cooperate on independent pathways to ensure efficient silencing of non-degenerated transposable elements. MET-2 mediates this in parallel to its role in repressing simple or tandem repeats.

Up-regulation of TEs in met-2;nrde-3 *correlates with embryonic lethality*

In earlier studies, we were surprised to see that *met-2*- and *met-2 set-25*-deficient embryos efficiently grew to adulthood, although they displayed severely compromised germline viability (Ahringer and Gasser 2018). While all *met-2* deficient strains showed significant sterility, organismal development of single and double *met-2 set-25* mutants was remarkably intact, with 88% of the double mutant embryos reaching adulthood (Zeller et al. 2016; Fig. 7E). Given the synergistic effects of *met*-2 and *nrde-3* on transposon derepression, we were curious to see how the *met-2;nrde-3* double mutant would influence embryonic survival and development.

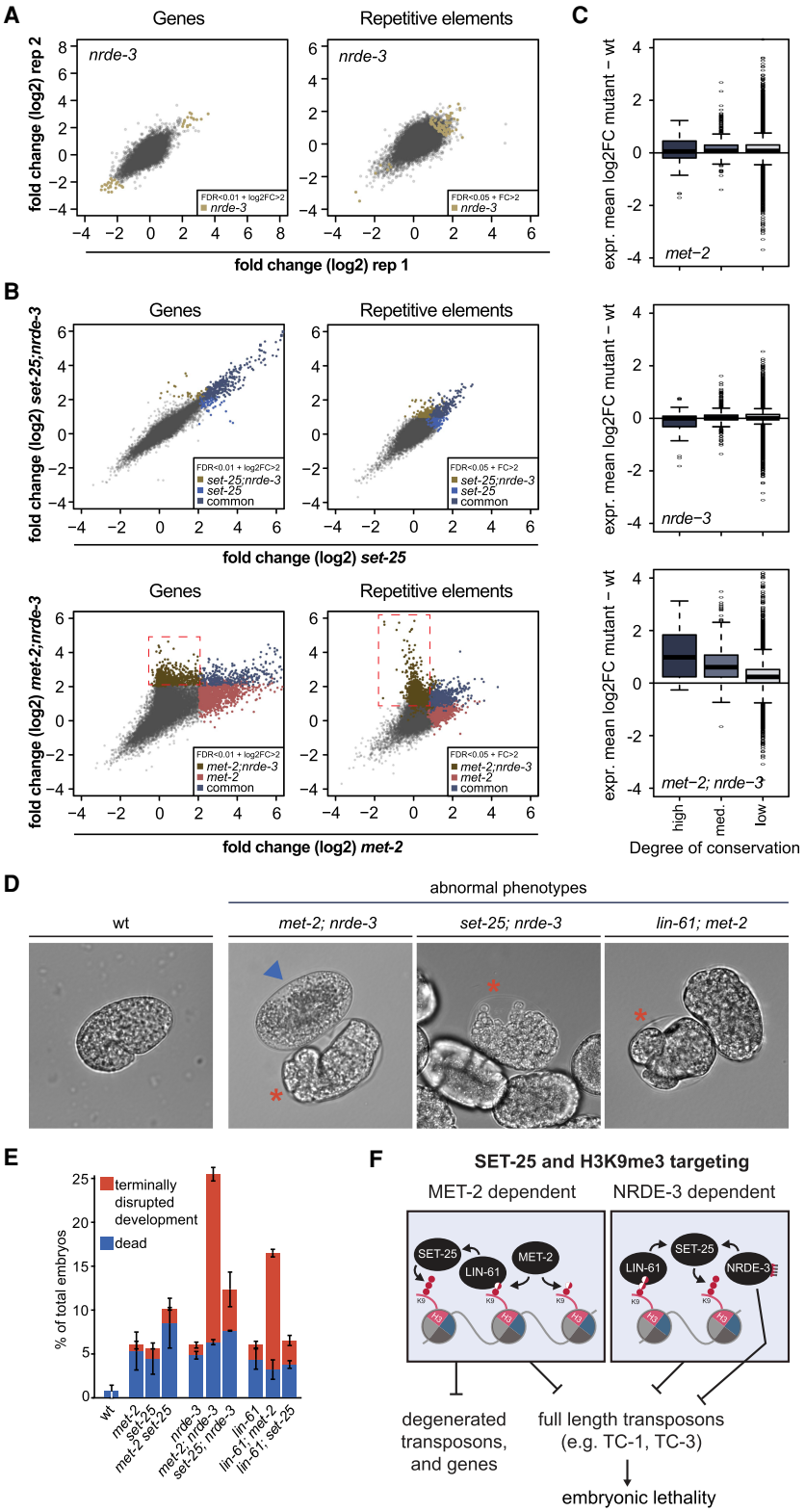

Figure 7. *met-2* and *nrde-3* loss leads to synergistic derepression of transposons and embryonic lethality. (*A*) Scatter plot of gene expression as $\log_2$ fold change over wt in early embryos of indicated mutants (two replicas shown, $N = 3$) at genes (*left* column) and repetitive elements (*right* column). Loci significantly changed are in color (genes: FDR 0.01 and $\log_2$ fold change >2 or <−2; repetitive elements: FDR 0.05 and fold change >2 or <−2). (*B*) Correlation between the fold change ($\log_2$) over wt for gene and repetitive element expression between *met-2* or *set-25* single and *met-2;nrde-3* and *set-25;nrde-3* double mutants. Loci significantly changed versus wt (genes: FDR 0.01 and $\log_2$ fold change >2 or <−2; repetitive elements: FDR 0.05 and fold change >2 or <−2) are colored according to the genotype. In dark purple are loci significantly changed in both genotypes. Genes and repetitive elements up-regulated only in *met-2;nrde-3* are boxed in red. (*C*) The mean $\log_2$ fold change in the indicated mutants over wt in expression of repetitive elements with a high, medium or low conservation score (based on DFAM bit score) in *met-2*, or *nrde-3* single and *met-2;nrde-3* double mutants. (*D*) Representative bright-field images of wt embryos showing normal development and *met-2;nrde-3*, *set-25;nrde-3*, and *lin-61;met-2* mutant embryos showing terminally disrupted development (red asterisk) and dead embryos (blue triangles). (*E*) Quantitation of percentage of dead embryos and embryos with a terminal disrupted development in wt, *met-2*, *set-25*, *met-2 set-25*, *nrde-3*, *met-2;nrde-3*, *set-25;nrde-3*, *lin-61*, *lin-61;met-2* and *lin-61;set-25* mutants at the *right* ($N = 3$, $n = 500$; error bars indicate SD).

When wt embryos are synchronized and plated, 99% progress through development without difficulty, hatching and producing fertile adults during standard laboratory growth at 20°C. In single mutants of *met-2*, *set-25*, *nrde-3*, or *lin-61*, around 5% of embryos were either dead or had a terminally disrupted development at an embryonic stage (Fig. 7D–E). Terminally disrupted development means that embryos became cellularized, but failed to develop into larvae, sometimes resembling balls of twitching muscle (see asterisks in Fig. 7D). Surprisingly, whereas the

met-2 set-25 double mutants showed ~10% lethality, in the *met-2;nrde-3* double mutant ~25% of embryos were either dead or had terminally disrupted development (Fig. 7D,E). This is the most lethal combination of H3K9me-modifying alleles that we have detected to date. As expected, the *lin-61;set-25* double mutant was epistatic with the *set-25* single mutant, while the *lin-61;met-2* double mutant was more lethal than *set-25*, yet the number of nonviable embryos laid did not increase. While the phenotypes in embryonic death are not highly revealing about the case of death, this result may indicate a more important role for LIN-61 in the soma, rather than in germline development.

Discussion

H3K9me is one of the few histone modifications that has been shown to promote self-propagation through the cell cycle, fulfilling an essential requirement for mitotic epigenetic inheritance (Audergon et al. 2015; Ragunathan et al. 2015b). We note, however, that de novo establishment of H3K9me2/me3 is necessary both to silence tissue-specific genes (Allshire and Madhani 2018; Nicetto et al. 2019) and to repress novel insertions of transposons in the genome (Leung et al. 2011). In this study we found two distinct pathways that distinguish the maintenance of somatic H3K9me3 from its nucleation (Fig. 7F). The H3K9me3 HMT SET-25, in contrast to MET-2, was able to silence a heterochromatic reporter de novo, which it did in a MET-2-independent manner. Intriguingly, MET-2-independent SET-25-modified loci account for only 13% of H3K9me3 loci in worms. The other 87% of the H3K9me3-loci stem from the sequential action of MET-2 and SET-25. Our studies show that the MET-2-independent targets of SET-25 are strongly enriched for intact DNA and RNA transposons, and exactly these conserved transposons are silenced by NRDE-3-dependent targeting of SET-25. In other words, the somatic Argonaute pathway that processes and binds RNA stemming from the locus represses the MET-2-independent SET-25 targets.

We note that in worms the majority of H3K9me3 marked loci show a stepwise mechanism of modification based on cooperation between the two HMTs (Towbin et al. 2012; Padeken et al. 2019). This is reminiscent of HMTs in mammals that maintain H3K9me3 at pericentric heterochromatin and at interspersed repetitive elements. SUV39h1 is essential for H3K9me3 at pericentric heterochromatin and a subset of nondegenerated LINE1 transposons (Peters et al. 2001; Bulut-Karslioglu et al. 2014). However, in SUV39h1/h2 double null mutants these sites retain H3K9me1 (Peters et al. 2003; Loyola et al. 2006), suggesting that monomethylation precedes the action of SUV39h. Exactly which enzyme generates the H3K9me1 mark in mammals remains unclear (Loyola et al. 2009; Pinheiro et al. 2012). In *C. elegans,* both SET-25 and MET-2 are able to place H3K9me1.

Unlike Su(var)3-9 in flies, SUV39h1/h2 in mammals or Clr4 in fission yeast (Allshire and Madhani 2018), *C. elegans* SET-25 does not possess a chromodomain that directly recognizes an existing H3K9me mark. Instead, the MBT domain protein LIN-61 appears to be the primary link between existing H3K9me and SET-25. The four MBT domains of LIN-61 have been shown to recognize all three methylation states of H3K9 (Koester-Eiserfunke and Fischle 2011), which makes it unique among the MBT domain proteins described in other species (Bonasio et al. 2010). This might explain why LIN-61 is equally important in the presence and absence of MET-2 to reinforce SET-25 targeting.

Precisely how LIN-61 reinforces SET-25 activity remains open, yet three mechanisms are consistent with our findings. First, LIN-61 could act indirectly. For instance, LIN-61 might recruit factors that remove active chromatin marks that could prevent SET-25 recruitment. These could be deacetylases, H3K4 demethylases, or chromatin remodelers. Second, SET-25 might simply bind LIN-61, serving as a bridge to the H3K9me1/me2 modified locus. Finally, the multiple me-binding domains within LIN-61 could cluster heterochromatin domains together to create a critical concentration of substrate in a small nuclear volume. This too might stimulate HMT activity (Bonasio et al. 2010). Although LIN-61 might have facilitated the spreading of H3K9me3, we saw no retraction of the borders of repressed chromatin domains in the *lin-61* mutant (Fig. 4G; Supplemental Fig. S3B), rendering this last option less likely. Although we were unable to show direct interaction between LIN-61 and SET-25 by pull-down, we do not exclude that they interact in vivo.

We note that the mammalian homolog of LIN-61, L3MBT2L (73% sequence similarity), interacts with the H3K9 HMT G9a, with HP1γ and with a noncanonical Polycomb repressive complex PRC1.6 (Ogawa et al. 2002; Trojer et al. 2011; Qin et al. 2012; Stielow et al. 2018). Given the similarity with SET-25, we suggest that the mammalian LIN-61 also serves to recruit H3K9 HMTs. This interaction is consistent with the defective developmental phenotypes that correlate with the loss of LIN-61 homologs in flies and mammals (Arai and Miyazaki 2005; Klymenko et al. 2006; Takada et al. 2007). In worms, the *lin-61;met-2* double mutant shows a higher rate of aberrant development than either single mutant or the *met-2 set-25* double mutant. Given that LIN-61 and L3MBTL2 have both been described as important for the repair of DNA damage (Johnson et al. 2013; Nowsheen et al. 2018). It is possible that the increased embryonic lethality in *lin-61;met-2* double mutants also reflects a failure to repair DNA damage induced by the promiscuous transcription of simple repeats in *met-2* mutants (Zeller et al. 2016; Padeken et al. 2019).

In contrast to LIN-61, we found that the somatic Argonaute NRDE-3 acts on a pathway that is entirely independent of MET-2 to specifically repress intact, nondegenerated transposons and, to a minor extent, genes. Remarkably, *nrde-3* deletion is highly synergistic with the loss of *met-2,* compromising the repression of its target REs (Fig. 7) and disrupting development (Fig. 7D–E). NRDE-3 is a somatic nuclear Argonaute that is essential for the shuttling of 22G RNAs from the cytoplasm to

the nucleus, facilitating their function in transcriptional silencing (Guang et al. 2008, 2010). Consistently, we observe enrichment of 22G RNAs arising from loci that retain SET-25 mediated H3K9me3 in *met-2* mutants. The enzyme that triggers the production of these specific 22G RNAs is not yet identified, although we also detected a partial loss of SET-25 targeting after knockdown of *ergo-1*, an Ago1 homolog. ERGO-1 acts upstream of NRDE-3 and is required for 22G RNA accumulation (Gent et al. 2010; Montgomery et al. 2012; Almeida et al. 2019a), suggesting that the ERGO-1 provides at least one of the triggers that results in transposon silencing.

We found an enrichment of small RNAs from H3K9me3 marked TEs both in wt and *met-2* mutant embryos, suggesting that silencing of nondegenerated transposons through H3K9me2/me3 is incomplete, and that residual transcripts are processed and bound by NRDE-3, even in wt cells. NRDE-3 in turn recruits SET-25, directly or indirectly, to impose transcriptional repression. This reinforcement pathway functions in wt as well as in *met-2* mutants, and the majority of transposons that retained H3K9me3 in *met-2* embryos lost H3K9me3 in the *met-2;nrde-3* double mutants.

We note that there is a small population of transposons that still carry H3K9me3 in the *met-2;nrde-3* double mutant, despite the complete dispersal of SET-25 foci. Given that NRDE-3 is a somatic Argonaute and that several distinct Argonautes act with the piRNA pathway in the *C. elegans* germline (Batista et al. 2008; Ashe et al. 2012; Lee et al. 2012; Shirayama et al. 2012), we do not exclude that a germline-specific Argonaute may enable SET-25 targeting prior to embryogenesis. Indeed, the *met-2 set-25* embryos show lower rates of death due to aberrant development than *nrde-3;met-2* embryos (Fig. 7D,E). One explanation may be that fewer fertilized embryos are generated in the *met-2 set-25* double mutant, which could mask "inviability" of laid embryos. Alternatively, NRDE-3 may have yet another role, for instance, contributing to transcript turnover during development independent of H3K9me3 deposition.

Taken together, we have shown that MET-2 catalyzed H3K9me1-2 and its MBT domain reader LIN-61 are crucial to maintain heterochromatin integrity, yet worms have layered additional pathways on top of this to ensure the repression of intact RNA and DNA transposons. Alongside the MET-2 pathway, NRDE-3 silences and nucleates heterochromatin at intact TEs "de novo" by recruiting SET-25 to sites of transposon expression. Whether this redundancy is more critical for existing genetic elements, or for novel inserts, is unclear. It would make sense that this small RNA pathway has evolved primarily to detect newly inserted transposons and recruit the enzymes necessary to silence them. This could explain why its loss is additive with that of the MET-2 repression pathway.

It remains controversial whether small RNAs contribute to silencing of repetitive elements in somatic cells in mammals (Czech et al. 2008; Kawamura et al. 2008), although they are shown to repress transposons in *Drosophila* (Ghildiyal et al. 2008). How that repression was achieved was not described. Interestingly it was recently shown that early establishment of heterochromatin in the two-cell stage mouse embryo is dependent on RNA from pericentromeric repeats and SUV39h2, although at that stage H3K9me3 is not correlated with repression, which is established later by SUV39h1 (Burton et al. 2020). These observations elevate the importance of the data presented here, as we show that a somatic Argonaute and its small RNA ligands establish and maintain H3K9me3, which indeed correlates with the transcriptional repression of intact TEs during somatic development in nematodes. This pathway escaped detection in the past because its loss is compensated for by MET-2/SETDB1 silencing mechanisms. In mammals such pathways may be further masked by DNA methylation (Estève et al. 2006; Du et al. 2015). By screening with the *C. elegans* met-2 mutant we could reveal the important role played by Argonaute-mediated targeting of the H3K9me3 HMT, SET-25, in somatic cells, where it represses nondegenerated transposons and stabilizes the genome. The loss of these redundant pathways of repression lead to significant death during embryonic development.

Materials and methods

Strains, transgenics, and RNAi

Caenorhabditis elegans strains were obtained from the *Caenorhabditis* Genome Center or were generated during this study (full description in Supplemental Table S1). Worms were grown on OP50 at 20°C if not otherwise stated.

Immunofluorescence (IF), antibodies, and live microscopy

IF was carried out as previously described (Zeller et al. 2016). Staining was performed in PBS + 0.1% Triton X-100. Primary antibodies were incubated in PBS + 0.1% TritonX-100 and 4% milk powder overnight at 4°C. Anti-pan-acetyl-H4 was included as a positive staining control (06-866, Merck Millipore, 1:500). For live cell imaging larvae were mounted on slides coated with 2% agarose. Microscopy was carried out on a spinning disc confocal microscope (Yokogawa X1 and a Yokogawa W1 scan head mounted on an Olympus and a Zeiss microscope respectively, Visitron, Puchheim). Stacks of images were analyzed using the KNIME analytics platform (Dietz and Berthold 2016). In summary, nuclei were detected using a seeded watershed segmentation, and foci detected using a Laplacian of Gaussian (LoG) detector from TrackMate (Tinevez et al. 2017; fmi-ij2-plugins-0.2.5 https://doi.org/10.5281/zenodo.1173536). Foci outside of a nucleus were ignored in the analysis.

Phenotypic characterization of embryonic lethality

Embryos were isolated from synchronized 1-d-old adult worms, cultured at 20°C and transferred onto microscope slides containing M9 buffer. Slides were scanned using a Olympus IX70 with bright-field illumination and phenotypes categorized according to morphology.

Chromatin IP (ChIP), RNA expression (RNA-seq and qPCR), and small RNA-seq

ChIP and RNA-seq were performed as previously described (Zeller et al. 2016). Libraries were prepared from chromatin IP and genomic DNA samples as described previously (Zeller et al. 2016). Read density along the genome was calculated by tiling the genome into 500-bp windows (nonoverlapping) and counting the number of sequence fragments within each window, using the qCount function of the QuasR package. To compensate for differences in the read depths, libraries were normalized to the total number of reads per library. ChIP-seq signals are displayed as average enrichment of IP – input (log2). For RNA-seq, total RNA was isolated and expression levels determined as previously described (Zeller et al. 2016). For small RNA-seq total small RNA was isolated using the Norgen single-cell RNA purification kit (51800). Purified small RNA was treated with 1 mlTAP (Lucigen) for 1 h at 37°C and libraries were prepared using QiaSeq miRNA library kit. See Supplemental Material for detailed description.

UV-RNA immunoprecipitation

Cells from synchronized embryos were dissociated into single cells by chitinase and mechanical shearing using syringe and 26G needle. RNA protein complexes were fixed with 0.15 J/cm^2 of UV and complexes precipitated using GFP-Trap Dynabeads (chromotek) overnight at 4°C. After purification and digestion by Proteinase K RNA abundance was quantified by RT-qPCR.

Data access

All data sets from this study have been uploaded to the Gene Expression Omnibus (GEO) under accession number GSE156551

Acknowledgments

We thank I. Katic and M. Guidi of the Friedrich Miescher Institute (FMI) for discussion and help with the generation of transgenic *C. elegans* strains. We thank S. Smallwood, E. Pandini Figueiredo Moreno, and S. Thiry from the FMI Genomics facilities for advice and discussion, and L. Gelman and J. Eglinger from the FMI Microscopy facility for advice on automated image analysis. Strains were provided by the *Caenorhabditis* Genetics Center (CGC), funded by National Institutes of Health Office of Research Infrastructure Programs (P40 OD010440). J.P. and S.M. were supported by a long-term EMBO fellowships. This project has received funding from the European Research Council (ERC) under the European Union's Horizon 2020 research and innovation program (Epiherigans grant agreement 743312 to S.M.G.). S.M.G. also thanks the Novartis Research Foundation for continued support.

Author contributions: J.P. planned and executed most experiments, evaluated results, and wrote the paper. S.M.G. planned experiments, evaluated results, and wrote the paper. S.M. planned and performed the immunofluorescence analysis. P.Z. helped to plan and execute the RNAi screen. C.E.D. helped with genetic crosses and biochemical analysis. V.K. provided invaluable technical help throughout.

References

Ahringer J, Gasser SM. 2018. Repressive chromatin in *Caenorhabditis elegans*: establishment, composition, and function. *Genetics* **208:** 491–511. doi:10.1534/genetics.117.300386

Allshire RC, Madhani HD. 2018. Ten principles of heterochromatin formation and function. *Nat Rev Mol Cell Biol* **19:** 229–244. doi:10.1038/nrm.2017.119

Almeida MV, Andrade-Navarro MA, Ketting RF. 2019a. Function and evolutions of nematode RNAi pathways. *Noncoding RNA* **5:** 8.

Almeida MV, de Jesus Domingues AM, Ketting RF. 2019b. Maternal and zygotic gene regulatory effects of endogenous RNAi pathways. *PLoS Genet* **15:** e1007784. doi:10.1371/journal.pgen.1007784

Arai S, Miyazaki T. 2005. Impaired maturation of myeloid progenitors in mice lacking novel Polycomb group protein MBT-1. *EMBO J* **24:** 1863–1873. doi:10.1038/sj.emboj.7600654

Ashe A, Sapetschnig A, Weick E-M, Mitchell J, Bagijn MP, Cording AC, Doebley A-L, Goldstein LD, Lehrbach NJ, Le Pen J, et al. 2012. piRNAs can trigger a multigenerational epigenetic memory in the germline of *C. elegans*. *Cell* **150:** 88–99. doi:10.1016/j.cell.2012.06.018

Audergon PNCB, Catania S, Kagansky A, Tong P, Shukla M, Pidoux AL, Allshire RC. 2015. Restricted epigenetic inheritance of H3K9 methylation. *Science* **348:** 132–135. doi:10.1126/science.1260638

Avgustinova A, Symeonidi A, Castellanos A, Urdiroz-Urricelqui U, Solé-Boldo L, Martín M, Pérez-Rodríguez I, Prats N, Lehner B, Supek F, et al. 2018. Loss of G9a preserves mutation patterns but increases chromatin accessibility, genomic instability and aggressiveness in skin tumours. *Nat Cell Biol* **20:** 1400–1409. doi:10.1038/s41556-018-0233-x

Bannister AJ, Zegerman P, Partridge JF, Miska EA, Thomas JO, Allshire RC, Kouzarides T. 2001. Selective recognition of methylated lysine 9 on histone H3 by the HP1 chromo domain. *Nature* **410:** 120–124. doi:10.1038/35065138

Batista PJ, Ruby JG, Claycomb JM, Chiang R, Fahlgren N, Kasschau KD, Chaves DA, Gu W, Vasale JJ, Duan S, et al. 2008. PRG-1 and 21U-RNAs interact to form the piRNA complex required for fertility in *C. elegans*. *Mol Cell* **31:** 67–78. doi:10.1016/j.molcel.2008.06.002

Becker JS, Nicetto D, Zaret KS. 2016. H3K9me3-dependent heterochromatin: barrier to cell fate changes. *Trends Genet* **32:** 29–41. doi:10.1016/j.tig.2015.11.001

Bessereau JL. 2006. Transposons in *C. elegans*. *WormBook* (ed. The *C. elegans* Research Community), WormBook, doi:10.1895/wormbook.1.70.1. http://www.wormbook.org.

Bonasio R, Lecona E, Reinberg D. 2010. MBT domain proteins in development and disease. *Semin Cell Dev Biol* **21:** 221–230. doi:10.1016/j.semcdb.2009.09.010

Bourque G, Burns KH, Gehring M, Gorbunova V, Seluanov A, Hammell M, Imbeault M, Izsvák Z, Levin HL, Macfarlan TS, et al. 2018. Ten things you should know about transposable elements. *Genome Biol* **19:** 199. doi:10.1186/s13059-018-1577-z

Bulut-Karslioglu A, De La Rosa-Velázquez IA, Ramirez F, Barenboim M, Onishi-Seebacher M, Arand J, Galán C, Winter GE, Engist B, Gerle B, et al. 2014. Suv39h-dependent H3K9me3 marks intact retrotransposons and silences LINE elements in mouse embryonic stem cells. *Mol Cell* **55:** 277–290. doi:10.1016/j.molcel.2014.05.029

Burkhart KB, Guang S, Buckley BA, Wong L, Bochner AF, Kennedy S. 2011. A pre-mRNA-associating factor links endogenous siRNAs to chromatin regulation. *PLoS Genet* **7:** e1002249. doi:10.1371/journal.pgen.1002249

Burton NO, Burkhart KB, Kennedy S. 2011. Nuclear RNAi maintains heritable gene silencing in *Caenorhabditis elegans*. *Proc*

Natl Acad Sci **108:** 19683–19688. doi:10.1073/pnas.1113310108

Burton A, Brochard V, Galan C, Ruiz-Morales ER, Rovira Q, Rodriguez-Terrones D, Kruse K, Le Gras S, Udayakumar VS, Chin HG, et al. 2020. Heterochromatin establishment during early mammalian development is regulated by pericentromeric RNA and characterized by non-repressive H3K9me3. *Nat Cell Biol* **22:** 767–778. doi:10.1038/s41556-020-0536-6

Carmell MA, Girard A, van de Kant HJ, Bourc'his D, Bestor TH, de Rooij DG, Hannon GJ. 2007. MIWI2 is essential for spermatogenesis and repression of transposons in the mouse male germline. *Dev Cell* **12:** 503–514. doi:10.1016/j.devcel.2007.03.001

Collins R, Cheng X. 2010. A case study in cross-talk: the histone lysine methyltransferases G9a and GLP. *Nucleic Acids Res* **38:** 3503–3511. doi:10.1093/nar/gkq081

Cox DN, Chao A, Baker J, Chang L, Qiao D, Lin H. 1998. A novel class of evolutionarily conserved genes defined by *piwi* are essential for stem cell self-renewal. *Genes Dev* **12:** 3715–3727. doi:10.1101/gad.12.23.3715

Czech B, Malone CD, Zhou R, Stark A, Schlingeheyde C, Dus M, Perrimon N, Kellis M, Wohlschlegel JA, Sachidanandam R, et al. 2008. An endogenous small interfering RNA pathway in *Drosophila*. *Nature* **453:** 798–802. doi:10.1038/nature07007

Daugherty AC, Yeo RW, Buenrostro JD, Greenleaf WJ, Kundaje A, Brunet A. 2017. Chromatin accessibility dynamics reveal novel functional enhancers in *C. elegans*. *Genome Res* **27:** 2096–2107. doi:10.1101/gr.226233.117

Delaney CE, Methot SP, Guidi M, Katic I, Gasser SM, Padeken J. 2019. Heterochromatic foci and transcriptional repression by an unstructured MET-2/SETDB1 co-factor LIN-65. *J Cell Biol* **218:** 820–838. doi:10.1083/jcb.201811038

Deniz Ö, Frost JM, Branco MR. 2019. Regulation of transposable elements by DNA modifications. *Nat Rev Genet* **20:** 417–431. doi:10.1038/s41576-019-0117-3

Dietz C, Berthold MR. 2016. KNIME for open-source bioimage analysis: a tutorial. *Adv Anat Embryol Cell Biol* **219:** 179–197. doi:10.1007/978-3-319-28549-8_7

Dodge JE, Kang Y-K, Beppu H, Lei H, Li E. 2004. Histone H3-K9 methyltransferase ESET Is essential for early development. *Mol Cellular Biology* **24:** 2478–2486. doi:10.1128/MCB.24.6.2478-2486.2004

Domansky AN, Kopantzev EP, Snezhkov EV, Lebedev YB, Leib-Mosch C, Sverdlov ED. 2000. Solitary HERV-K LTRs possess bi-directional promoter activity and contain a negative regulatory element in the U5 region. *FEBS Lett* **472:** 191–195. doi:10.1016/S0014-5793(00)01460-5

Du J, Johnson LM, Jacobsen SE, Patel DJ. 2015. DNA methylation pathways and their crosstalk with histone methylation. *Nat Rev Mol Cell Biol* **16:** 519–532. doi:10.1038/nrm4043

Dunn CA, Romanish MT, Gutierrez LE, van de Lagemaat LN, Mager DL. 2006. Transcription of two human genes from a bidirectional endogenous retrovirus promoter. *Gene* **366:** 335–342. doi:10.1016/j.gene.2005.09.003

Elgin SC, Reuter G. 2013. Position-effect variegation, heterochromatin formation, and gene silencing in *Drosophila*. *Cold Spring Harb Perspect Biol* **5:** a017780. doi:10.1101/cshperspect.a017780

Estève P-O, Chin HG, Smallwood A, Feehery GR, Gangisetty O, Karpf AR, Carey MF, Pradhan S. 2006. Direct interaction between DNMT1 and G9a coordinates DNA and histone methylation during replication. *Genes Dev* **20:** 3089–3103. doi:10.1101/gad.1463706

Feuchter A, Mager D. 1990. Functional heterogeneity of a large family of human LTR-like promoters and enhancers. *Nucleic Acids Res* **18:** 1261–1270. doi:10.1093/nar/18.5.1261

Fischer T, Cui B, Dhakshnamoorthy J, Zhou M, Rubin C, Zofall M, Veenstra TD, Grewal SI. 2009. Diverse roles of HP1 proteins in heterochromatin assembly and functions in fission yeast. *Proc Natl Acad Sci* **106:** 8998–9003. doi:10.1073/pnas.0813063106

Garrigues JM, Sidoli S, Garcia BA, Strome S. 2015. Defining heterochromatin in *C. elegans* through genome-wide analysis of the heterochromatin protein 1 homolog HPL-2. *Genome Res* **25:** 76–88. doi:10.1101/gr.180489.114

Gent JI, Lamm AT, Pavelec DM, Maniar JM, Parameswaran P, Tao L, Kennedy S, Fire AZ. 2010. Distinct phases of siRNA synthesis in an endogenous RNAi pathway in *C. elegans* soma. *Mol Cell* **37:** 679–689. doi:10.1016/j.molcel.2010.01.012

Ghandi M, Huang FW, Jané-Valbuena J, Kryukov GV, Lo CC, McDonald ER, Barretina J, Gelfand ET, Bielski CM, Li H, et al. 2019. Next-generation characterization of the cancer cell line encyclopedia. *Nature* **569:** 503–508. doi:10.1038/s41586-019-1186-3

Ghildiyal M, Seitz H, Horwich MD, Li C, Du T, Lee S, Xu J, Kittler ELW, Zapp ML, Weng Z, et al. 2008. Endogenous siRNAs derived from transposons and mRNAs in *Drosophila* somatic cells. *Science* **320:** 1077–1081. doi: 10.1126/science.1157396.

Grishok A, Sinskey JL, Sharp PA. 2005. Transcriptional silencing of a transgene by RNAi in the soma of *C. elegans*. *Genes Dev* **19:** 683–696. doi:10.1101/gad.1247705

Gu W, Shirayama M, Conte D, Vasale J, Batista PJ, Claycomb JM, Moresco JJ, Youngman EM, Keys J, Stoltz MJ, et al. 2009. Distinct argonaute-mediated 22G-RNA pathways direct genome surveillance in the *C. elegans* germline. *Mol Cell* **36:** 231–244. doi:10.1016/j.molcel.2009.09.020

Gu SG, Pak J, Guang S, Maniar JM, Kennedy S, Fire A. 2012. Amplification of siRNA in *Caenorhabditis elegans* generates a transgenerational sequence-targeted histone H3 lysine 9 methylation footprint. *Nat Genet* **44:** 157–164. doi:10.1038/ng.1039

Guang S, Bochner AF, Pavelec DM, Burkhart KB, Harding S, Lachowiec J, Kennedy S. 2008. An Argonaute transports siRNAs from the cytoplasm to the nucleus. *Science* **321:** 537–541. doi:10.1126/science.1157647

Guang S, Bochner AF, Burkhart KB, Burton N, Pavelec DM, Kennedy S. 2010. Small regulatory RNAs inhibit RNA polymerase II during the elongation phase of transcription. *Nature* **465:** 1097–1101. doi:10.1038/nature09095

Holoch D, Moazed D. 2015. RNA-mediated epigenetic regulation of gene expression. *Nat Rev Genet* **16:** 71–84. doi:10.1038/nrg3863

Horard B, Eymery A, Fourel G, Vassetzky N, Puechberty J, Roizes G, Lebrigand K, Barbry P, Laugraud A, Gautier C, et al. 2009. Global analysis of DNA methylation and transcription of human repetitive sequences. *Epigenetics* **4:** 339–350. doi:10.4161/epi.4.5.9284

Houwing S, Kamminga LM, Berezikov E, Cronembold D, Girard A, van den Elst H, Filippov DV, Blaser H, Raz E, Moens CB, et al. 2007. A role for Piwi and piRNAs in germ cell maintenance and transposon silencing in Zebrafish. *Cell* **129:** 69–82. doi:10.1016/j.cell.2007.03.026

Hubley R, Finn RD, Clements J, Eddy SR, Jones TA, Bao W, Smit AFA, Wheeler TJ. 2016. The Dfam database of repetitive DNA families. *Nucleic Acids Res* **44:** D81–D89. doi:10.1093/nar/gkv1272

Jachowicz JW, Bing X, Pontabry J, Bošković A, Rando OJ, Torres-Padilla M-E. 2017. LINE-1 activation after fertilization regulates global chromatin accessibility in the early mouse embryo. *Nat Genet* **49:** 1502–1510. doi:10.1038/ng.3945

Johnson NM, Lemmens BB, Tijsterman M. 2013. A role for the malignant brain tumour (MBT) domain protein LIN-61 in DNA double-strand break repair by homologous recombination. *PLoS Genet* **9:** e1003339. doi:10.1371/journal.pgen.1003339

Kawamura Y, Saito K, Kin T, Ono Y, Asai K, Sunohara T, Okada TN, Siomi MC, Siomi H. 2008. *Drosophila* endogenous small RNAs bind to Argonaute 2 in somatic cells. *Nature* **453:** 793–797. doi:10.1038/nature06938

Khristich AN, Mirkin SM. 2020. On the wrong DNA track: molecular mechanisms of repeat-mediated genome instability. *J Biol Chem* **295:** 4134–4170. doi:10.1074/jbc.REV119.007678

Klein SJ, O'Neill RJ. 2018. Transposable elements: genome innovation, chromosome diversity, and centromere conflict. *Chromosome Res* **26:** 5–23. doi:10.1007/s10577-017-9569-5

Klymenko T, Papp B, Fischle W, Köcher T, Schelder M, Fritsch C, Wild B, Wilm M, Müller J. 2006. A polycomb group protein complex with sequence-specific DNA-binding and selective methyl-lysine-binding activities. *Genes Dev* **20:** 1110–1122. doi:10.1101/gad.377406

Koester-Eiserfunke N, Fischle W. 2011. H3k9me2/3 binding of the MBT domain protein LIN-61 is essential for *Caenorhabditis elegans* vulva development. *PLoS Genet* **7:** e1002017. doi:10.1371/journal.pgen.1002017

Kuramochi-Miyagawa S, Kimura T, Yomogida K, Kuroiwa A, Tadokoro Y, Fujita Y, Sato M, Matsuda Y, Nakano T. 2001. Two mouse piwi-related genes: miwi and mili. *Mech Dev* **108:** 121–133. doi:10.1016/S0925-4773(01)00499-3

Kuramochi-Miyagawa S, Kimura T, Ijiri TW, Isobe T, Asada N, Fujita Y, Ikawa M, Iwai N, Okabe M, Deng W, et al. 2004. Mili, a mammalian member of piwi family gene, is essential for spermatogenesis. *Development* **131:** 839–849. doi:10.1242/dev.00973

Lachner M, O'Carroll D, Rea S, Mechtler K, Jenuwein T. 2001. Methylation of histone H3 lysine 9 creates a binding site for HP1 proteins. *Nature* **410:** 116–120. doi:10.1038/35065132

Lee HC, Gu W, Shirayama M, Youngman E, Conte D Jr., Mello CC. 2012. *C. elegans* piRNAs mediate the genome-wide surveillance of germline transcripts. *Cell* **150:** 78–87. doi:10.1016/j.cell.2012.06.016

Leung DC, Dong KB, Maksakova IA, Goyal P, Appanah R, Lee S, Tachibana M, Shinkai Y, Lehnertz B, Mager DL, et al. 2011. Lysine methyltransferase G9a is required for de novo DNA methylation and the establishment, but not the maintenance, of proviral silencing. *Proc Natl Acad Sci* **108:** 5718–5723. doi:10.1073/pnas.1014660108

Lin H, Spradling AC. 1997. A novel group of pumilio mutations affects the asymmetric division of germline stem cells in the *Drosophila* ovary. *Development* **124:** 2463–2476.

Loyola A, Bonaldi T, Roche D, Imhof A, Almouzni G. 2006. PTMs on H3 variants before chromatin assembly potentiate their final epigenetic state. *Mol Cell* **24:** 309–316. doi:10.1016/j.molcel.2006.08.019

Loyola A, Tagami H, Bonaldi T, Roche D, Quivy JP, Imhof A, Nakatani Y, Dent SY, Almouzni G. 2009. The HP1α-CsAF1-SetDB1-containing complex provides H3K9me1 for Suv39-mediated K9me3 in pericentric heterochromatin. *EMBO Rep* **10:** 769–775. doi:10.1038/embor.2009.90

Luo S, Lu J. 2017. Silencing of transposable elements by piRNAs in *Drosophila*: an evolutionary perspective. *Genomics Proteomics Bioinformatics* **15:** 164–176. doi:10.1016/j.gpb.2017.01.006

Matsui T, Leung D, Miyashita H, Maksakova IA, Miyachi H, Kimura H, Tachibana M, Lorincz MC, Shinkai Y. 2010. Proviral silencing in embryonic stem cells requires the histone methyltransferase ESET. *Nature* **464:** 927–931. doi:10.1038/nature08858

Mattout A, Gaidatzis D, Padeken J, Schmid CD, Aeschimann F, Kalck V, Gasser SM. 2020. LSM2-8 and XRN-2 contribute to the silencing of H3K27me3-marked genes through targeted RNA decay. *Nat Cell Biol* **22:** 579–590. doi:10.1038/s41556-020-0504-1

McMurchy AN, Stempor P, Gaarenstroom T, Wysolmerski B, Dong Y, Aussianikava D, Appert A, Huang N, Kolasinska-Zwierz P, Sapetschnig A, et al. 2017. A team of heterochromatin factors collaborates with small RNA pathways to combat repetitive elements and germline stress. *Elife* **6:** e21666.

Meister P, Towbin BD, Pike BL, Ponti A, Gasser SM. 2010. The spatial dynamics of tissue-specific promoters during *C. elegans* development. *Genes Dev* **24:** 766–782. doi:10.1101/gad.559610

Montgomery TA, Rim YS, Zhang C, Dowen RH, Phillips CM, Fischer SE, Ruvkun G. 2012. PIWI associated siRNAs and piRNAs specifically require the *Caenorhabditis elegans* HEN1 ortholog henn-1. *PLoS Genet* **8:** e1002616. doi:10.1371/journal.pgen.1002616

Motamedi MR, Verdel A, Colmenares SU, Gerber SA, Gygi SP, Moazed D. 2004. Two RNAi complexes, RITS and RDRC, physically interact and localize to noncoding centromeric RNAs. *Cell* **119:** 789–802. doi:10.1016/j.cell.2004.11.034

Nakayama J, Rice JC, Strahl BD, Allis CD, Grewal SI. 2001. Role of histone H3 lysine 9 methylation in epigenetic control of heterochromatin assembly. *Science* **292:** 110–113. doi:10.1126/science.1060118

Nicetto D, Donahue G, Jain T, Peng T, Sidoli S, Sheng L, Montavon T, Becker JS, Grindheim JM, Blahnik K, et al. 2019. H3K9me3-heterochromatin loss at protein-coding genes enables developmental lineage specification. *Science* **363:** 294–297. doi:10.1126/science.aau0583

Nowsheen S, Aziz K, Aziz A, Deng M, Qin B, Luo K, Jeganathan KB, Zhang H, Liu T, Yu J, et al. 2018. L3MBTL2 orchestrates ubiquitin signalling by dictating the sequential recruitment of RNF8 and RNF168 after DNA damage. *Nat Cell Biol* **20:** 455–464. doi:10.1038/s41556-018-0071-x

Ogawa H, Ishiguro K, Gaubatz S, Livingston DM, Nakatani Y. 2002. A complex with chromatin modifiers that occupies E2F- and Myc-responsive genes in G0 cells. *Science* **296:** 1132–1136. doi:10.1126/science.1069861

Ozata DM, Gainetdinov I, Zoch A, O'Carroll D, Zamore PD. 2019. PIWI-interacting RNAs: small RNAs with big functions. *Nature Rev Genet* **20:** 89–108. doi:10.1038/s41576-018-0073-3

Padeken J, Zeller P, Gasser SM. 2015. Repeat DNA in genome organization and stability. *Curr Opin Genet Dev* **31:** 12–19. doi:10.1016/j.gde.2015.03.009

Padeken J, Zeller P, Towbin B, Katic I, Kalck V, Methot SP, Gasser SM. 2019. Synergistic lethality between BRCA1 and H3K9me2 loss reflects satellite derepression. *Genes Dev* **33:** 436–451. doi:10.1101/gad.322495.118

Pak J, Fire A. 2007. Distinct populations of primary and secondary effectors during RNAi in *C. elegans*. *Science* **315:** 241–244. doi:10.1126/science.1132839

Palazzo A, Lorusso P, Miskey C, Walisko O, Gerbino A, Marobbio CMT, Ivics Z, Marsano RM. 2019. Transcriptionally promiscuous 'blurry' promoters in Tc1/mariner transposons allow transcription in distantly related genomes. *Mob DNA* **10:** 13. doi:10.1186/s13100-019-0155-6

Payer LM, Burns KH. 2019. Transposable elements in human genetic disease. *Nat Rev Genet* **20:** 760–772. doi:10.1038/s41576-019-0165-8

Peters AH, O'Carroll D, Scherthan H, Mechtler K, Sauer S, Schöfer C, Weipoltshammer K, Pagani M, Lachner M, Kohlmaier A, et al. 2001. Loss of the Suv39h histone methyltransferases impairs mammalian heterochromatin and genome stability. *Cell* **107:** 323–337. doi:10.1016/S0092-8674(01)00542-6

Peters AHFM, Kubicek S, Mechtler K, O'Sullivan RJ, Derijck AAHA, Perez-Burgos L, Kohlmaier A, Opravil S, Tachibana M, Shinkai Y, et al. 2003. Partitioning and plasticity of repressive histone methylation states in mammalian chromatin. *Mol Cell* **12:** 1577–1589. doi:10.1016/S1097-2765(03)00477-5

Pinheiro I, Margueron R, Shukeir N, Eisold M, Fritzsch C, Richter FM, Mittler G, Genoud C, Goyama S, Kurokawa M, et al. 2012. Prdm3 and Prdm16 are H3K9me1 methyltransferases required for mammalian heterochromatin integrity. *Cell* **150:** 948–960. doi:10.1016/j.cell.2012.06.048

Qin J, Whyte WA, Anderssen E, Apostolou E, Chen HH, Akbarian S, Bronson RT, Hochedlinger K, Ramaswamy S, Young RA, et al. 2012. The polycomb group protein L3mbtl2 assembles an atypical PRC1-family complex that is essential in pluripotent stem cells and early development. *Cell Stem Cell* **11:** 319–332. doi:10.1016/j.stem.2012.06.002

Ragunathan K, Jih G, Moazed D. 2015a. Epigenetic inheritance uncoupled from sequence-specific recruitment. *Science* **348:** 1258699. doi:10.1126/science.1258699

Ragunathan K, Jih G, Moazed D. 2015b. Epigenetic inheritance uncoupled from sequence-specific recruitment. *Science* **348:** 1258699. doi:10.1126/science.1258699

Raizada MN, Benito M-I, Walbot V. 2001. The MuDR transposon terminal inverted repeat contains a complex plant promoter directing distinct somatic and germinal programs. *Plant J* **25:** 79–91.

Reinberg D, Vales LD. 2018. Chromatin domains rich in inheritance. *Science* **361:** 33–34. doi:10.1126/science.aat7871

Rodríguez-Paredes M, Esteller M. 2011. Cancer epigenetics reaches mainstream oncology. *Nat Med* **17:** 330–339. doi:10.1038/nm.2305

Rowbotham SP, Li F, Dost AFM, Louie SM, Marsh BP, Pessina P, Anbarasu CR, Brainson CF, Tuminello SJ, Lieberman A, et al. 2018. H3k9 methyltransferases and demethylases control lung tumor-propagating cells and lung cancer progression. *Nat Commun* **9:** 4559. doi:10.1038/s41467-018-07077-1

Rowe HM, Jakobsson J, Mesnard D, Rougemont J, Reynard S, Aktas T, Maillard PV, Layard-Liesching H, Verp S, Marquis J, et al. 2010. KAP1 controls endogenous retroviruses in embryonic stem cells. *Nature* **463:** 237–240. doi:10.1038/nature08674

Shankar SR, Bahirvani AG, Rao VK, Bharathy N, Ow JR, Taneja R. 2013. G9a, a multipotent regulator of gene expression. *Epigenetics* **8:** 16–22. doi:10.4161/epi.23331

Shirayama M, Seth M, Lee H-C, Gu W, Ishidate T, Conte D, Mello Craig C. 2012. piRNAs initiate an epigenetic memory of nonself RNA in the *C. elegans* germline. *Cell* **150:** 65–77. doi:10.1016/j.cell.2012.06.015

Sijen T, Steiner FA, Thijssen KL, Plasterk RHA. 2007. Secondary siRNAs result from unprimed RNA synthesis and form a distinct class. *Science* **315:** 244–247. doi:10.1126/science.1136699

Slotkin RK, Martienssen R. 2007. Transposable elements and the epigenetic regulation of the genome. *Nat Rev Genet* **8:** 272–285. doi:10.1038/nrg2072

Soufi A, Donahue G, Zaret KS. 2012. Facilitators and impediments of the pluripotency reprogramming factors' initial engagement with the genome. *Cell* **151:** 994–1004. doi:10.1016/j.cell.2012.09.045

Sridharan R, Gonzales-Cope M, Chronis C, Bonora G, McKee R, Huang C, Patel S, Lopez D, Mishra N, Pellegrini M, et al. 2013. Proteomic and genomic approaches reveal critical functions of H3K9 methylation and heterochromatin protein-1γ in reprogramming to pluripotency. *Nat Cell Biol* **15:** 872–882. doi:10.1038/ncb2768

Stielow B, Finkernagel F, Stiewe T, Nist A, Suske G. 2018. MGA, L3MBTL2 and E2F6 determine genomic binding of the non-canonical polycomb repressive complex PRC1.6. *PLoS Genet* **14:** e1007193. doi:10.1371/journal.pgen.1007193

Sugiyama T, Cam H, Verdel A, Moazed D, Grewal SIS. 2005. RNA-dependent RNA polymerase is an essential component of a self-enforcing loop coupling heterochromatin assembly to siRNA production. *Proc Natl Acad Sci* **102:** 152–157. doi:10.1073/pnas.0407641102

Tachibana M, Sugimoto K, Nozaki M, Ueda J, Ohta T, Ohki M, Fukuda M, Takeda N, Niida H, Kato H, et al. 2002. G9a histone methyltransferase plays a dominant role in euchromatic histone H3 lysine 9 methylation and is essential for early embryogenesis. *Genes Dev* **16:** 1779–1791. doi:10.1101/gad.989402

Takada Y, Isono K, Shinga J, Turner JM, Kitamura H, Ohara O, Watanabe G, Singh PB, Kamijo T, Jenuwein T, et al. 2007. Mammalian Polycomb Scmh1 mediates exclusion of polycomb complexes from the XY body in the pachytene spermatocytes. *Development* **134:** 579–590. doi:10.1242/dev.02747

Tinevez JY, Perry N, Schindelin J, Hoopes GM, Reynolds GD, Laplantine E, Bednarek SY, Shorte SL, Eliceiri KW. 2017. Trackmate: an open and extensible platform for single-particle tracking. *Methods* **115:** 80–90. doi:10.1016/j.ymeth.2016.09.016

Torrano J, Al Emran A, Hammerlindl H, Schaider H. 2019. Emerging roles of H3K9me3, SETDB1 and SETDB2 in therapy-induced cellular reprogramming. *Clin Epigenetics* **11:** 43. doi:10.1186/s13148-019-0644-y

Tóth KF, Pezic D, Stuwe E, Webster A. 2016. The piRNA pathway guards the germline genome against transposable elements. *Adv Exp Med Biol* **886:** 51–77. doi:10.1007/978-94-017-7417-8_4

Towbin BD, González-Aguilera C, Sack R, Gaidatzis D, Kalck V, Meister P, Askjaer P, Gasser SM. 2012. Step-wise methylation of histone H3K9 positions heterochromatin at the nuclear periphery. *Cell* **150:** 934–947. doi:10.1016/j.cell.2012.06.051

Trojer P, Cao AR, Gao Z, Li Y, Zhang J, Xu X, Li G, Losson R, Erdjument-Bromage H, Tempst P, et al. 2011. L3MBTL2 protein acts in concert with PcG protein-mediated monoubiquitination of H2A to establish a repressive chromatin structure. *Mol Cell* **42:** 438–450. doi:10.1016/j.molcel.2011.04.004

van den Beek M, da Silva B, Pouch J, Ali Chaouche MEA, Carré C, Antoniewski C. 2018. Dual-layer transposon repression in

heads of *Drosophila melanogaster*. *RNA* **24:** 1749–1760. doi:10.1261/rna.067173.118

Vastenhouw NL, Fischer SE, Robert VJ, Thijssen KL, Fraser AG, Kamath RS, Ahringer J, Plasterk RH. 2003. A genome-wide screen identifies 27 genes involved in transposon silencing in *C. elegans*. *Curr Biol* **13:** 1311–1316. doi:10.1016/S0960-9822(03)00539-6

Wallis DC, Nguyen DAH, Uebel CJ, Phillips CM. 2019. Visualization and quantification of transposon activity in *Caenorhabditis elegans* RNAi pathway mutants. *G3* **9:** 3825.

Wolf D, Goff SP. 2009. Embryonic stem cells use ZFP809 to silence retroviral DNAs. *Nature* **458:** 1201–1204. doi:10.1038/nature07844

Yamada T, Fischle W, Sugiyama T, Allis CD, Grewal SIS. 2005. The nucleation and maintenance of heterochromatin by a histone deacetylase in fission yeast. *Mol Cell* **20:** 173–185. doi:10.1016/j.molcel.2005.10.002

Yang N, Kazazian HH. 2006. L1 retrotransposition is suppressed by endogenously encoded small interfering RNAs in human cultured cells. *Nat Struct Mol Biol* **13:** 763–771. doi:10.1038/nsmb1141

Zeller P, Padeken J, van Schendel R, Kalck V, Tijsterman M, Gasser SM. 2016. Histone H3K9 methylation is dispensable for *Caenorhabditis elegans* development but suppresses RNA:DNA hybrid-associated repeat instability. *Nat Genet* **48:** 1385–1395. doi:10.1038/ng.3672

Zhang K, Mosch K, Fischle W, Grewal SI. 2008. Roles of the Clr4 methyltransferase complex in nucleation, spreading and maintenance of heterochromatin. *Nat Struct Mol Biol* **15:** 381–388. doi:10.1038/nsmb.1406